TU Delft

Delft University of Technology

Quantum dot solar cells

Small beginnings have large impacts

Ganesan, Abiseka Akash; Houtepen, Arjan J.; Crisp, Ryan W.

DOI
10.3390/app8101867

Publication date
2018

Document Version
Final published version

Published in
Applied Sciences (Switzerland)

Citation (APA)
Ganesan, A. A., Houtepen, A. J., & Crisp, R. W. (2018). Quantum dot solar cells: Small beginnings have large impacts. *Applied Sciences (Switzerland)*, *8*(10), Article 1867. https://doi.org/10.3390/app8101867

Important note
To cite this publication, please use the final published version (if applicable).
Please check the document version above.

Copyright
Other than for strictly personal use, it is not permitted to download, forward or distribute the text or part of it, without the consent of the author(s) and/or copyright holder(s), unless the work is under an open content license such as Creative Commons.

Takedown policy
Please contact us and provide details if you believe this document breaches copyrights.
We will remove access to the work immediately and investigate your claim.

This work is downloaded from Delft University of Technology.
For technical reasons the number of authors shown on this cover page is limited to a maximum of 10.

applied sciences

MDPI

Review

Quantum Dot Solar Cells: Small Beginnings Have Large Impacts

Abiseka Akash Ganesan, Arjan J. Houtepen and Ryan W. Crisp *

Department of Chemical Engineering, Delft University of Technology, Van der Maasweg 9, 2629HZ Delft, The Netherlands; abisekaakash@gmail.com (A.A.G.); A.J.Houtepen@tudelft.nl (A.J.H.)
* Correspondence: R.W.Crisp@tudelft.nl; Tel.: +31-15-27-82173

Received: 31 August 2018; Accepted: 26 September 2018; Published: 10 October 2018

Featured Application: Solution-processed optoelectronic nanomaterials for use in lighting, energy-harvesting, and sensing.

Abstract: From a niche field over 30 years ago, quantum dots (QDs) have developed into viable materials for many commercial optoelectronic devices. We discuss the advancements in Pb-based QD solar cells (QDSCs) from a viewpoint of the pathways an excited state can take when relaxing back to the ground state. Systematically understanding the fundamental processes occurring in QDs has led to improvements in solar cell efficiency from ~3% to over 13% in 8 years. We compile data from ~200 articles reporting functioning QDSCs to give an overview of the current limitations in the technology. We find that the open circuit voltage limits the device efficiency and propose some strategies for overcoming this limitation.

Keywords: quantum dots; lead sulfide; solar cells; photovoltaics; IV-VI semiconductors; nanocrystals; solution-processed; ligand-exchange

1. Introduction

Colloidal semiconductor quantum dots (QDs) are nanometer-sized crystals made and suspended in solution. Because they can be processed in solution, have facilely tunable properties, and demonstrate unique photophysics, they are intriguing for optoelectronic devices, imaging, and fundamental science. The size and size distribution of the QD ensemble matter because they directly control the energy levels of the material (i.e., the highest occupied molecular orbital to the lowest unoccupied molecular orbital (HOMO-LUMO) gap or band gap). This observation can be explained from two points of view. The first viewpoint is a bottom-up description where the combination of molecular orbitals (energy states) with each additional atom bonded to the QD narrow the HOMO-LUMO gap until there is a negligible change, resulting in the "bulk" material. In the second top-down viewpoint, spatially confining the exciton (a bound electron-hole pair) wavefunction by making a crystal smaller thereby increases the energy required to excite the QD (e.g., the bandgap), analogous to the particle-in-a-box description [1,2].

There are several ways to synthesize colloidal QDs, which are reviewed elsewhere [3–9]. The main method, hot injection, follows a reaction pathway as described by La Mer's model of nucleation and growth [10]. After injection, the precursor concentration in solution increases and exceeds the nucleation threshold (i.e., the solution is supersaturated); at this point, a burst of nucleation occurs and continues along with QD growth until the precursor concentration drops below the nucleation threshold and enters the growth regime. During growth, size focusing can occur if the QD growth rate is size-dependent, i.e., if smaller QDs grow faster than larger ones then the size distribution will narrow. During this time however, the high surface energy of small QDs drives their dissolution

and precipitation onto larger QDs leading to an increase in the size distribution—A process called Ostwald's ripening [5,11]. Influencing these processes by reaction temperature, precursor reactivity, and/or reaction kinetics allows for control over the size and size-distribution [12–23]. Once all the reactants are used and the concentration approaches zero, the growth regime ends. Typically, around half of the QD's atoms reside at the surface [24,25]. With such a high ratio of atoms exposed at the surface versus in the core, it is not surprising that surface chemistry and surface environment dominate many properties of QDs—not just by size alone [26].

With these two factors in mind (the size and the surface), this Review sheds light upon photoexcitations in colloidal semiconductor QD films and devices, from absorption to extraction (and the time between). We start with a brief overview of the processes that occur at each time scale ranging from a few femtoseconds to microseconds before giving an in-depth discussion of the progress of Pb-based QD solar cells (QDSCs). For in-depth discussions on each subtopic, we refer the interested readers to more specific reviews [27–41].

2. Timescales of Excited State Processes

In the sections below, we discuss the possible processes that occur when a QD absorbs a photon. A detailed understanding of each of these processes and their relevant timescales, shown in Figure 1, enables rational design of optoelectronic devices. We highlight various device studies that apply the lessons learned in each process to give an overall view of the history and state-of-the-art of Pb-based QDSCs.

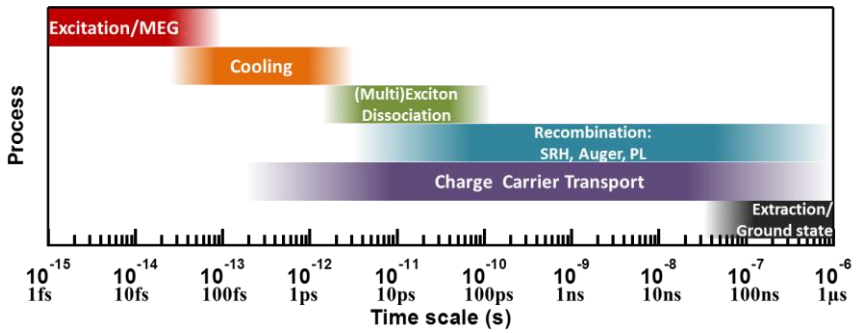

Figure 1. Schematic outline showing the different timescales of the processes in the lifetime of a photoexcitation.

2.1. Absorption and Multiple Exciton Generation

Propagation and absorption of light in QD materials is the critical first step in using QDs in optoelectronics. As discussed by Leatherdale et al. [42] and Ricard et al. [43], the absorption cross section can be written as:

$$\sigma = \frac{\omega}{n_s' c} |f(\omega)|^2 2 n_1 k_1 \left(\frac{4}{3} \pi a^3 \right) \quad (1)$$

where ω is the angular frequency of light, c is the speed of light, n_s' is the complex refractive index ($n_s' = n_s - ik_s$) of the solvent or surrounding medium (s subscript), $2n_1k_1 = \alpha$ is the absorption coefficient of the bulk material (1 subscript), a is the radius of the particles, k is the extinction coefficient, and the local field factor $f(\omega)$ is given by:

$$f(\omega) = \frac{3 n_s'^2}{n_1'^2 + 2 n_s'^2} \quad (2)$$

The overall absorption in a film of QDs can be increased by changing these properties. Increased light absorption in a solar cell typically increases the total electrical current and thus power produced. However, as we will discuss in the section on charge transport, the total film thickness for the highest

efficiency devices does not fully absorb the incident light. Therefore strategies to improve this without increasing the film thickness were developed. Research groups have shown evidence of the positive impact of using plasmonic materials incorporated in QDSCs. By placing materials with a localized surface plasmon resonance (LSPR) [44] in the QDSC, the absorption, due to the higher local field factor, increased. Gold (Au) nano-shells [45], silver (Ag) nano-cubes [46], Au/Ag core/shell nano-cubes [47], and also a combination of Au bipyramids and nano-spheres [48] have been tested in QDSCs. Figure 2a shows the effect of incorporating Au nanoshells into PbS QD films. In each case, it was observed that there was an enhancement in the photocurrent due to an increase in light absorption in the near infra-red (IR) region of the solar spectrum close to the first exciton peak and also in different parts of the spectrum based on the position of the plasmonic nanocrystals (NCs). Alternatively to the PbS and PbSe QDs limited to the IR spectral region, Hg-chalcogenide QDs have spectral features and optoelectronic properties that extend into the far-IR and THz regions [49,50]. Using plasmonic gold nanorods with HgTe QDs [51], gold nanodisk arrays with HgSe QDs [52] and HgTe QDs [53] improved the photocurrent extraction demonstrating the broad applicability of this absorption enhancement strategy.

Another technique used to increase light absorption is the use of nanostructured electrodes or engineer the device layers to have constructive interference of the incident light [54–57]. These electrodes reflect the incident light back into the absorber layer such that the effective path length of the light wave inside the absorber layer increases as depicted in Figure 2b. In solar cells with thin absorber layers arising from small minority carrier diffusion lengths, increasing the path length of the incident light wave through the absorber material by promoting multiple passes increases the probability of light absorption in the thin film thereby improving device performance. While this technique is difficult to implement in QDSCs due to the uneven accumulation of QD solution in the textured metal oxide electrodes during spin-coating/dip-coating [58,59], Sargent's group has optimized the steps involved in texturing to help overcome this limitation giving rise to high-performance devices [60–62].

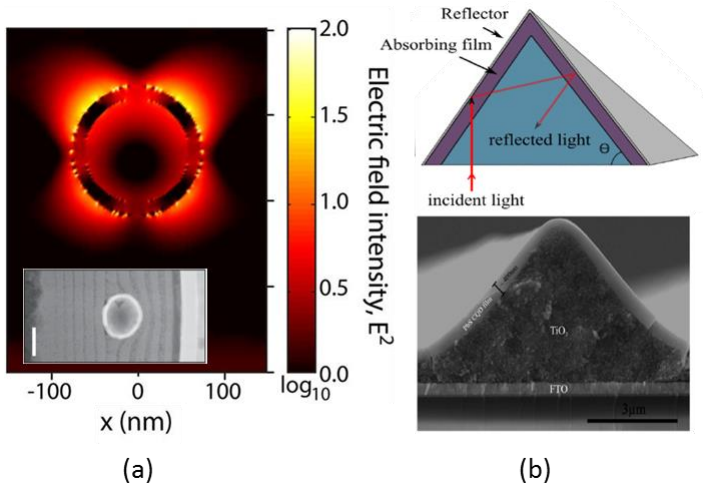

Figure 2. (**a**) A plot between the electric field intensity (E^2) and distance x from the center of the nano-shell (x-axis) shows an increase in the intensity of the electric field only near the nano-shell surface. Inset: a cross-sectional transmission electron microscopic snapshot (TEM—FEI Titan 80–300, Hillsboro, OR, USA) of the incorporation of the nano-shell inside the PbS layer. Adapted with permission from reference [45], copyright 2013 American Chemical Society. (**b**) A schematic (top) and a scanning electron microscope (SEM—FEI, Hillsboro, Oregon, USA) image (bottom) showing the nanostructured QDSCs with several internal reflections of the incident light. Adapted with permission from reference [62], copyright 2015 American Chemical Society.

Hens and Moreels [63] rewrite (1) and (2) as the absorption coefficient μ for a dispersion of QDs with volume fraction f as:

$$\mu = \frac{n_1}{n_s}|f(\omega)|^2 f\alpha \quad (3)$$

This clearly shows the high sensitivity of the absorption coefficient to the surrounding environment (n_1/n_s), which includes the surface ligation of the QDs. For instance, titrating *p*-methylbenzenethiolate into a solution of PbS QDs leads to a broadband increase in absorption and a bathochromic shift of the first exciton transition peak [64]. This result is surprising given the fact that *p*-methylbenzenethiolate shows negligible absorption in the spectral region of interest and, more interestingly, calculating the change in $f(\omega)$ defined by the Maxwell-Garnet effective medium theory does not predict the ~340% increase in the molar absorption coefficient at 400 nm indicating that the synergistic effect of ligand/QD system is greater than the simple sum of the two. Mixing of the molecular orbitals of the ligand/QD system, calculated using density functional theory, shows an increase in the density of states near the band edge, increasing the number of allowed transitions, thus enhancing the absorption of light. Ligands, such as these, affecting the QD electronic structure have been termed 'non-innocent' ligands and provide a tool for microscopic control of macroscopic properties [65–67]. While these specific ligand complexes have not yet been applied to devices, they could hold promise for increasing the overall absorption of QDSCs. Further ordering of the QDs into a superlattice has also shown up to 5 fold enhancement of the absorption and represents a potential method to improving device properties as we discuss in the final section [68,69]. Other strategies include hybrid structures between organic conductors and QDs, as discussed elsewhere [70–73].

In addition to how strongly a QD absorbs light, the size of the QD determines the photon energy that can be absorbed to create an exciton. If the absorbed photon has energy greater than twice the bandgap (i.e., $\hbar\omega > 2E_g$), then the excitons have multiple paths to decay to their ground state energy levels, each of which occurs over a characteristic timescale. The possibility of an Auger pathway (green arrows, pathway 2a in Figure 3) in QD semiconductors also opens doors to the possibility of an inverse Auger pathway as shown in pathway 1a of Figure 3. Auger processes are three-body events where one carrier interacts with another carrier of opposite charge and transfers energy to a third carrier. The photoexcitation by a high energy photon ($\hbar\nu$ at least $> 2E_g$) can cause the high energy electron-hole pair to split into two or more electron-hole pairs of lesser energy. The first pathway we will discuss is multiple exciton generation (MEG) also referred to as carrier multiplication (CM) in cases where the excitations yield free charges. This phenomenon was observed in QDs at much lower bandgap multiples as compared to bulk semiconductors [74–78]. Known as impact ionization (II) in bulk semiconductors, CM was observed to be of significance only at photon energies far into the UV range (>3 eV) which contributes to less than 1% of the solar spectrum. This is because the strong coupling of electron and phonon states in bulk semiconductors provides a quicker cooling pathway for hot carriers through phonon emission (schematically represented by the red wavy lines in pathway 1b of Figure 3) and the need for the crystal lattice momentum conservation raises the threshold energy required for CM. The quantum confinement of charge carriers in QDs however has been expected to help overcome these limitations. Due to the small crystal size and quantum confinement along all three dimensions in QDs, the need for crystal momentum conservation is minimized while these discrete energy levels separated by multiple optical phonon energies makes the relaxation of hot carriers via phonon emission a rather slow process.

Furthermore, MEG is a carrier scattering process mediated via the carriers' Coulomb interaction. As this Coulomb interaction is enhanced due to confinement of the electron and hole wavefunctions in QDs, the rate of CM is also increased [77]. The possibility of using the multiple excitons to produce higher photocurrents has motivated researchers to use such QD semiconductors in solar cells [79–81]. However, in addition to the generation of multiple excitons, the effective separation of the exciton into charge carriers and their extraction into electron- and hole-accepting contacts are equally important in realizing the true potential of MEG-based solar cells [82]. Using time-resolved microwave conductivity (TRMC) measurements, Aerts et al. [83] showed that varying the excitation energy and measuring the photoconductance leads to a signal that correlates directly to the fraction of absorbed photons (i.e., the mobility was constant as a function of excitation energy but the number of free carriers depends on the fraction of photons absorbed). At excitation energies above $2E_g$, the yield of carriers

exceeded 100% indicating that free charges were produced through CM (pathway 2b of Figure 3). These excess charges can also be used to drive chemical reactions (not just solar cells) with yields greater than 100% [84].

One concept to increase the efficiency of CM is through band alignment engineering [85]. By combining different materials in a quasi-type II heterojunction (e.g., PbSe/CdSe core/shell QDs), the carrier cooling rate can be reduced so the MEG rate becomes proportionally more dominant and the MEG yield thus increases [86]. However, one drawback of this approach is that the hole is effectively stuck in the core of the QD and not free to move to contacts precluding applications requiring long-range carrier transport. Alternatively to core/shell nanocrystals, Janus particles (anisotropic particles where each side of the particle is a different material) could retain the same benefits while allowing access to each carrier. Nanayakkara et al. have shown a built-in potential difference in these heterostructured nanocrystals with scanning Kelvin probe measurements that can be explained by having a space-charge region where 10–15 charges have transferred across the nanoscale junction [87,88]. Furthermore, Zhang et al. [89] report a controllable cation exchange synthesis to produce Janus particles of various PbE and CdE (E = S, Se, Te) compositions that have been applied to this type of study [90]. More simplistically, Grimaldi et al. [91] fabricated films of mixed CdSe/PbSe QDs and observed hot-electron transfer between the QDs indicating the energy states of neighboring QDs are coupled.

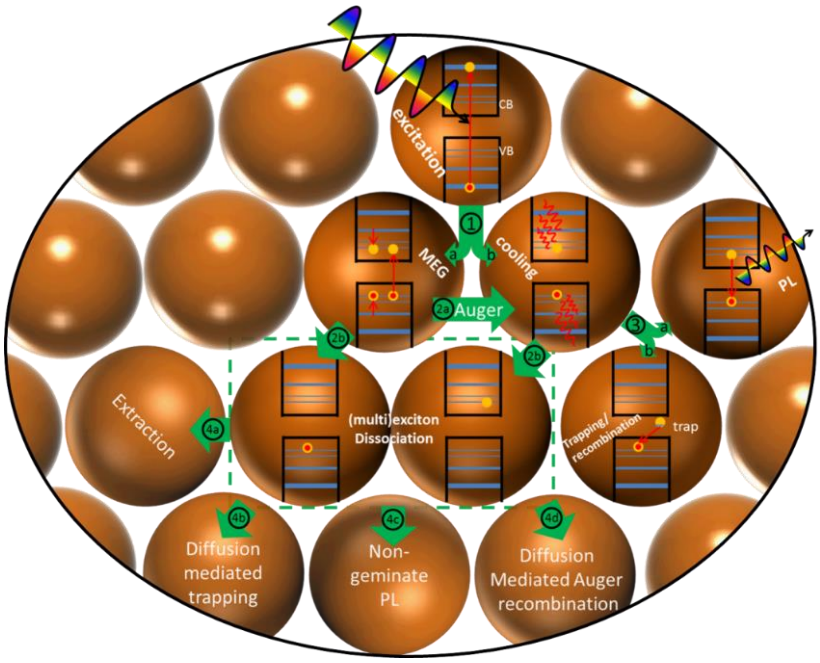

Figure 3. Schematic representations of the different steps in creating free charges in QD films. Green arrows are the different pathways the excitation can take, red arrows represent energy changes either phonon emission, photoluminescence, or Auger/inverse Auger energy transfer, blue lines represent the quantized states in the potential well (black lines) of the QDs (brown spheres), yellow dots are electrons and yellow circles with red dots are holes.

Further understanding and control via wavefunction engineering, opens up many new possibilities to employ advanced photophysics to applied optoelectronic devices. For instance, the exciton can spatially delocalize over the surrounding QDs if the energy landscape is favorable. Metal chalcogenide complexes, namely In_2Te_3 and $[In_2Se_4]^{2-}$, as QD ligands lead to excitons delocalized over six nearest neighbor QDs measured using a cross-polarized transient grating spectroscopy, which is a four-wave mixing experiment that diffracts the probe signal off a grating of excitons that decays through fine structure relaxation, influenced by the spin-flip rate [92]. The longer-lived signal directly correlates to

a larger exciton size [93]. Using organic ligands that reduce the QD-QD spacing does not lead to the exciton delocalization; on this time scale, the QDs are effectively isolated. Only if the QDs are necked or fused by thermal annealing do the authors report similar delocalization for organically ligated QDs. This clearly leads to a situation where the QDs are "confined-but-connected" [94] and has large impacts on charge carrier dynamics as discussed in the next sections.

2.2. Cooling

One pathway the electron and/or hole can take to decay to their ground state energy first involves thermalizing or "cooling" to the band edges emitting excess energy as phonons. Energy lost through cooling is the largest loss-mechanism for lower-bandgap solar cells with unabsorbed photons being the largest loss for higher-bandgap materials. There are several strategies to overcome this limitation including MEG (discussed above), tandem solar cells [95–98], and hot-carrier extraction [41,91,99]. Due to quantum confinement, the available energy states of electrons and holes are discrete and energetically separated by an amount of energy larger than the energy of a single optical phonon. Simultaneously emitting multiple phonons is an unfavorable process; therefore, carrier cooling should be considerably slowed leading to what is known as a phonon bottleneck [100,101]. However, experiments show far less than the predicted slow carrier cooling time, indicating other energy-loss processes are occurring, possibly through coupling to the vibrational modes of the surface ligands [102,103]. C-O, C-H, and O-H vibrations are at energies comparable to the energy level spacing in QDs (e.g., 10 s to 100 s of meV). A systematic exploration of the carrier cooling rates as a function of ligand moieties with different vibrational spectra has not been done but would shed light on the absence of this interesting phenomenon.

While the quantization of energy levels in QDs is expected to reduce the electron-phonon coupling due to significant differences in electron and phonon energies, recent studies have shown otherwise. Bozyigit et al. [104] quantitatively show the existence of higher energy phonon states that arise due to the mechanical softness of the QD surface where atoms vibrate with higher amplitudes than the core atoms. These results show the existence of a higher electron-phonon coupling that provides a quick path for hot electron cooling as opposed to the initial hypothesis of the existence of a phonon bottleneck. Recently the same group showed theoretically that such soft surface phonon modes indeed enhance electron and hole cooling in PbS QDs [105].

Another process known as Auger cooling allows for the transfer of energy between the excited electron and hole which can cool more efficiently due to the closer energy spacing of the valence band states in many QD materials [106–108]. Now that these processes are better understood, work can be done in designing ways to overcome the challenges. Perhaps incasing the QDs in a solid matrix to minimize the QD surface vibration and, if the matrix is conductive, transport the charge carriers away from each other before multi-exciton processes can occur—as discussed next.

2.3. Charge Carrier Transport

There are several proposed mechanisms for how charges can be transported in nanocrystalline systems; these include: nearest neighbor hopping, variable range hopping (VRH), Efros-Shklovskii VRH (ES-VRH), co-tunneling, and Bloch transport (band-like transport), which are discussed extensively in the literature and reviewed by Talapin et al. [30], Guyot-Sionnest [33], and Kagan et al. [27]. Here we will focus on the nearest neighbor hopping of charge carriers between QDs. We chose to focus on this particular mechanism because it is the dominate transport mechanism for many of the QD solids used in solar cells. Given all the sources of disorder in a film of QDs (energy disorder caused by different sizes of QDs, different spacing and crystal orientation between QDs, variation in impurities in each QD, variation in ligand coverage, etc.) it is unlikely band-like transport or other long-range transport are the dominant energy transfer mechanisms, unless the QDs are extremely strongly coupled by significant necking or, potentially, by semiconducting inorganic ligands [33,109]. For QD films used

in solar cells this strong coupling is usually not the case. Using the Einstein-Smoluchowski relation, we can derive the hopping rate ($\Gamma_{hop,e+h} = 1/\tau_{hop}$) [110]:

$$\Gamma_{hop,e+h} = \frac{k_B T \cdot \Sigma\mu \cdot NN}{e\Delta^2} \quad (4)$$

where k_B is the Boltzmann constant, T the temperature, $\Sigma\mu$ is the sum of the electron and hole mobility, NN is the number of nearest neighbors (12 in a hexagonal close-packed structure), e the elementary charge, and Δ is the hopping distance. Because the ligands used to grow and disperse the QDs are long, they are exchanged with shorter ligands to improve carrier transport by lowering Δ [111]. Using transient absorption techniques, Gao et al. [110] observed fast spectral diffusion of photoexcited carriers as carriers hopped to the largest QDs (i.e., those with the lowest bandgap) that is complete in ~2 ps. One design of a QDSC uses this concept as a "quantum funnel" where the authors layered different sizes of QDs to tune the energy landscape and drive charges to the contacts [112,113]. One downside to this is that Gao et al. [114] observed that due to this fast hopping to larger QDs, Auger recombination can be efficient even at low excitation fluence. This is due to multiple carriers congregating in the largest QDs and implies that because energy disorder in QD solids leads to enhanced recombination it can be used for optical gain or fast optical switching [114]. Other groups have since improved the Monte Carlo approach used in these initial studies to analyze the nature of charge transport in QD films [115–117]. Surface ligands play a strong role as they induce both positional and energetic disorder that lowers the mobility and/or lifetime of photoexcited carriers [71,118]. As coupling between QDs is increased, the electron and hole wavefunctions delocalize over the QD solid. An Anderson transition occurs as transport goes from thermally activated hopping (due to wavefunction localization caused by electronic disorder) to band-like transport where the mobility increases with decreasing temperature due to reduced phonon scattering [119–121].

Solar cells exhibiting external quantum efficiencies (EQE) over 100% from CM first employed two different ligand treatments of ethane dithiol (EDT) and hydrazine [79]; without this bilayer structure (discussed more below) CM was not observed in completed devices. In a subsequent study by Davis et al. [80], they also used EDT/hydrazine scheme to show improved extraction with PbSe nanorods (NRs), while PbTe QDs interestingly only required 3-mercaptopropionic acid (MPA) to exhibit CM with over 120% [81]. Sandeep et al. [122] showed a strong correlation between the mobility of a QD solid and the CM yield for PbSe QDs by controllably varying the coupling of the QDs with alkyl diamines of different carbon-chain length. This L-promoted Z-type ligand displacement leads to necking of the QDs thereby increasing the charge carrier mobility [69,123]. This result gives a simple design rule that to exploit CM in devices, charge carrier mobility should be in the order of 1 cm^2/Vs [124].

However, with increased mobility, the charge carrier lifetime often decreases due to the increased trapping and recombination rates—this is known as the "mobility-invariant regime" [125]. Therefore, the design and engineering of QDSCs should take into account the diffusion length of changes, not just the mobility [126–128]. This lesson also applies to other colloidal QD materials and application, such as Hg-chalcogenide QDs where improvements in photodetection and photovoltaics are possible through increased understanding of the role of the surface chemistry on trapping and recombination [129,130].

2.4. (Multi)Exciton Dissociation

Dissociation can be thought of as a special case of charge transport where one half of the exciton (either the electron or hole) has to overcome an additional energy barrier before transferring to another QD, i.e., from the Miller-Abrams rate [131]: $\Gamma_{dis} = \Gamma_{hop,e+h} \cdot e^{E_{dis}/k_B T}$. This additional energy barrier is the exciton binding energy. As discussed by Talgorn et al. [119] and Delerue [132], this energy

needed for dissociation, E_{dis}, involves the Coulomb interaction and the cross-polarization energy, expressed as [132]:

$$E_{dis} = \frac{1.79e^2}{4\pi\varepsilon_0\varepsilon_{in}} + \frac{e^2}{4\pi\varepsilon_0 R}\frac{\varepsilon_{in} - \varepsilon_{out}}{\varepsilon_{in}\varepsilon_{out}} \quad (5)$$

with ε_0 the vacuum permittivity, R the QD radius, e the elementary charge and ε_{in} and ε_{out} the relative permittivities in the QD and outside the QD, respectively. The physical interpretation of the cross-polarization energy can be understood using the method of image charges. Each charge has a virtual mirror charge outside the QD that can be thought of as a sum of partial induced charges arising from the dielectric nature of the surrounding medium. Here again, the surface chemistry of the QD plays a role in determining the ε_{out} value, which is a measure of the dielectric polarizability. The surrounding film/media that the exciton dissociates into is effectively a mixture of ligands and other QDs; therefore, ε_{out} can be calculated given a certain volume fraction, f, via the Bruggeman effective medium approximation taking ligands and QDs into account [119,133]:

$$f\frac{\varepsilon_{in} - \varepsilon_{out}}{\varepsilon_{in} + \kappa\varepsilon_{out}} = (f-1)\frac{\varepsilon_{ligand} - \varepsilon_{out}}{\varepsilon_{ligand} + \kappa\varepsilon_{out}} \quad (6)$$

It is an interesting question whether the values for ε_{in} and ε_{ligand} should be taken as the static relative permittivity or the high frequency relative permittivity. Intuitively one could consider an exciton a static entity; however, associated with the exciton is an angular frequency as in a classical picture the electron and hole orbit each other. Hence the relevant frequency is determined by the angular frequency of the exciton. Therefore, it is most appropriate to use the higher frequency permittivity if the angular frequency of the exciton is commensurate with that of the optical phonons of the material [114]. For a quantum confined charge carrier, the confinement energy is a kinetic energy and also corresponds to the charge moving around at some frequency in the QD. While the details are beyond the scope of this review, the upshot is that for excitons, and or charges in quantum confined materials in general it is more appropriate to use the high frequency optical dielectric constant. As an example, PbSe QDs with 1,2-ethanediamine ligands E_{dis} using the low frequency (i.e., static) relative permittivities for the QD and ligands yields around 10 meV, whereas, calculating the E_{dis} with the relative permittivity at optical frequencies gives around 80 meV [69,114]. The latter value has been confirmed experimentally [134].

2.5. Recombination

Carriers can recombine radiatively (emitting a photon—Figure 3, pathway 3a) or nonradiatively (emitting phonon(s)). For nonradiative recombination there are two main mechanisms by which charges recombine: Auger recombination (Figure 3, pathway 2a) and Shockley-Read-Hall (SRH) recombination (Figure 3, pathway 3b). The PL quantum yield (QY) is determined by the competition between these processes and greatly depends on the surface chemistry because this effects SRH recombination via the passivation of surface traps [135].

Nonradiative recombination via SHR, also known as trap-assisted recombination, is the main energy loss mechanism at low-excitation density for QD solids applied to optoelectronic devices namely solar cells and photodetectors as the PLQY is <50% in electronically coupled QD solids and Auger recombination is only efficient at high fluences [114,136–138]. This type of recombination is typically only dominant when there is a high density of carriers (as in high power LEDs) and is responsible for the "droop" in LED efficiency at higher powers [139].

Marshall et al. [140] employed a metathesis (cation-exchange) reaction to synthesize PbS QDs from CdS QDs. They found that cation-exchanged PbS have a lower trap density than "conventionally" (directly) synthesized PbS QDs. This is the first report to demonstrate bimolecular radiative recombination that is reasonably competitive with trap-assisted recombination in electronically coupled QD films. In conventionally synthesized QDs, electronic coupling leads to a complete quenching of the PL at room

temperature as photoexcited charges diffuse to traps and recombine nonradiatively. This foreshadowed the surge of breakthroughs in solar cell PCE with halide ligand passivation strategies.

Another special case of recombination is stimulated emission that forms the basis for lasing. Many QD materials have energy levels such that a population inversion can occur and lead to amplified spontaneous emission [141–143].

2.6. Extraction

Ultimately, the charges that do not recombine in the QD solid need to be extracted. Surface chemistry of the QDs plays a strong role in the extraction efficiency in QD devices. By using different ligands, the relative energy levels (Fermi level (EF), valence band maximum (VBM), and conduction band minimum (CBM)) of the QD solid can be varied and therefore used to create an asymmetry in the device energy levels [144,145]. An asymmetry is necessary for a device to keep the electrons and holes spatially separated, limiting recombination, and selectively extracting charge carriers at the different contacts. This not only applies to solar cells but also photodetectors. While we focus mainly on Pb-chalcogenides the Hg-chalcogenides are also of interests to increase the spectral range from the near-IR to the far-IR and THz regions [146,147]. The following section details the history and progression of QDSCs using many of the concepts described above to manage the flow of energy in devices.

3. Quantum Dot Solar Cells

A better understanding of the physics of QDs and the development of efficient methods of QD synthesis paved the way for their implementation in light harvesting devices (photodiodes and solar cells) and light emitting devices (Lasers and LEDs). For light-harvesting devices, PbS has emerged as the most promising candidate among the different QD materials due to its large light absorption coefficient, large Bohr radius, and facile band gap tunability [148].

The design or structure of a QDSC dictates many of its performance parameters [39,40,149–151]. Three structures are shown in Figure 4. The rightmost structure of Figure 4 shows QD sensitized solar cells (based on dye-sensitized solar cells [152]) that were first fabricated using an n-type mesoporous TiO_2 (m-TiO_2) sensitized with PbS QDs. The first report from Hoyer et al. [153] described photoconduction in a device with a bandgap of ≈1.85 eV where the QD energy bands aligned favorably with that of the cathode enabling carrier extraction from the QDs. Adding to this work, Ju et al. [154] developed PV cells showing a power conversion efficiency (PCE) of 3% by sandwiching the above setup between tin-doped indium oxide (ITO) and gold. However, the disadvantages of the mesoporous structure for sensitized cells with liquid electrolytes pushed QDSCs towards planar solid-state configurations. Nonetheless, research on sensitized solar cells continued with the development of a technique known as successive ion layer adsorption and reaction (SILAR) to synthesize PbS QDs in situ on m-TiO_2. This technique involves dipping a photoelectrode (TiO_2) coated substrate successively in precursor solutions containing the Pb^{2+} and S^{2-} ions to get PbS QDs. This deposition method, known to pack a higher density of PbS QDs in the pores of m-TiO_2, promotes higher light absorption and charge extraction at the interface between TiO_2 and PbS QDs and hence has improved device performance. All solid-state sensitized cells, without any polysulphide electrolyte, have also been fabricated using TiO_2 NRs similar to a bulk heterojunction used by organic photovoltaics [155]. This has opened interesting avenues of research to achieve higher performance QD-sensitized cells [156–159]. Other notable achievements include devices with Hg^{2+} doped PbS QDs made through the SILAR method with exceptionally high photocurrents of 30 mA/cm^2 [160] and devices using PbS/CdS core/shell QDs that exhibit PCEs greater than 7% [161]. We limit our discussion to Pb-based QDs; however, there is a burgeoning area of research using other QD materials as the sensitizers with over 12% PCE using Zn-Cu-In-Se (ZCISe) QDs [162–165].

To overcome the shortcomings of a QD-sensitized configuration, planar junction devices were developed, starting with a Schottky junction. A Schottky junction QDSC uses the work function

difference between the QDs and a metal contact to generate a photovoltage that extracts charges as shown in the leftmost structure of Figure 4. Prior work [166–169] has shown the presence of a Schottky junction at the QD/metal contact interface leading to charge separation at the rear boundary which introduces a limitation to this configuration if the diffusion length is not long enough for charges to reach the junction. The increased probability of recombination of charge carriers excited farther away from the junction by shorter wavelength photons reduces the produced photocurrent and limits the thickness of the device to below the point where not all the photons greater than the bandgap are absorbed. Additionally, Schottky junctions have a practical limit on the maximum open circuit voltage (V_{OC}). The maximum V_{OC} is approximately ½ the bandgap; limited mainly because of the high reverse saturation current and photocurrent limited by the standard AM1.5 irradiance (higher V_{OC} is possible under concentrated light) [170,171].

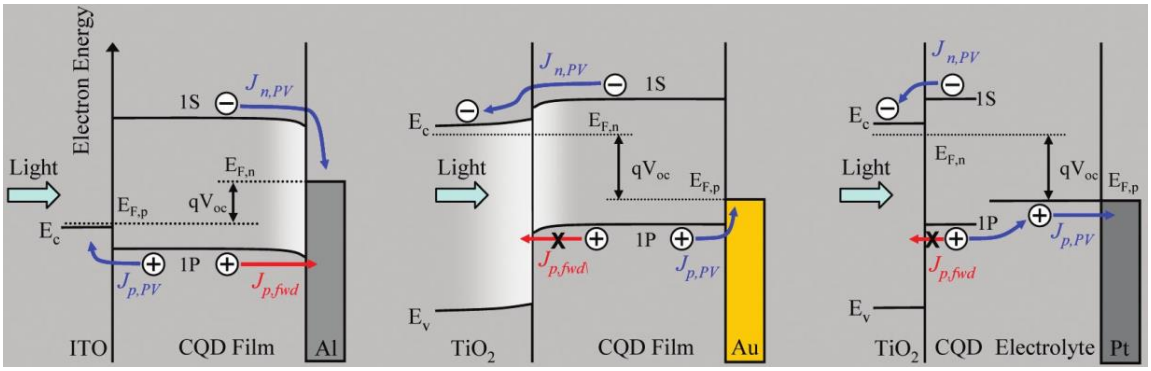

Figure 4. A compilation of the band diagrams of the three common PbS QDSCs configurations. The leftmost configuration depicts a Schottky junction solar cell where charge carrier separation and extraction occur at the rear junction, between the PbS QD layer and the metal electrode. The middle configuration shows a depleted heterojunction solar cell in which the TiO_2 nanoparticles-PbS QD layer interface forms the main junction where charge extraction and separation takes place. The rightmost configuration shows a QD-sensitized device in which the differences in electron affinity between the TiO_2 and the PbS QD layer causes charge separation. Reproduced with permission from reference [172], copyright 2010 American Chemical Society.

To overcome the limitations posed by Schottky junction cells, planar p-n heterojunction solar cells were developed (middle structure of Figure 4) and are the current front-runner for the highest efficiency devices. Finding the proper band alignment is critical to maximizing the PCE in a heterojunction solar cell. In this regard, ligands play a large role in determining the conduction band (CB), valence band (VB), Fermi energy levels by inducing a dipole moment on the QD surface. Brown et al. [145] compared the effects of 12 different ligands on the energy levels of PbS QDs and concluded that a dipole moment formed at the interface between the ligand and the QD surface combined with the intrinsic dipole moment of different ligands shifts the energy levels of the QD by different magnitudes. Following this, other research groups have also performed similar spectroscopy studies on QDs under inert and ambient conditions to determine the effect of different ligands and processing conditions on the energy levels of PbS QDs [173]. Figure 5 shows a compilation of UPS and XPS measurements of the band positions of 29 different ligands on PbS QDs.

Furthermore, density functional theory (DFT) calculations have shown that the lack of an intrinsic dipole moment in iodide ligands lead to deeper energy level shifts. Thiols, with higher intrinsic dipole moments, cancel out the interface dipole moment created by ligand interaction with the QD surface leading to a shallower energy level shift. This has formed the basis for band alignment engineering leading to high-efficiency PV cells [174].

While ligands have played the role of dopants, QD films have also been doped using remote doping techniques. Kirmani et al. [175] showed that based on the electron affinity and ionization energies, dopants with a deep electron affinity induce a remote flow of electrons from the VBM of

the QD into the LUMO of the dopant to leave behind a p-doped QD (with the reverse energy flow yielding n-doped QDs).

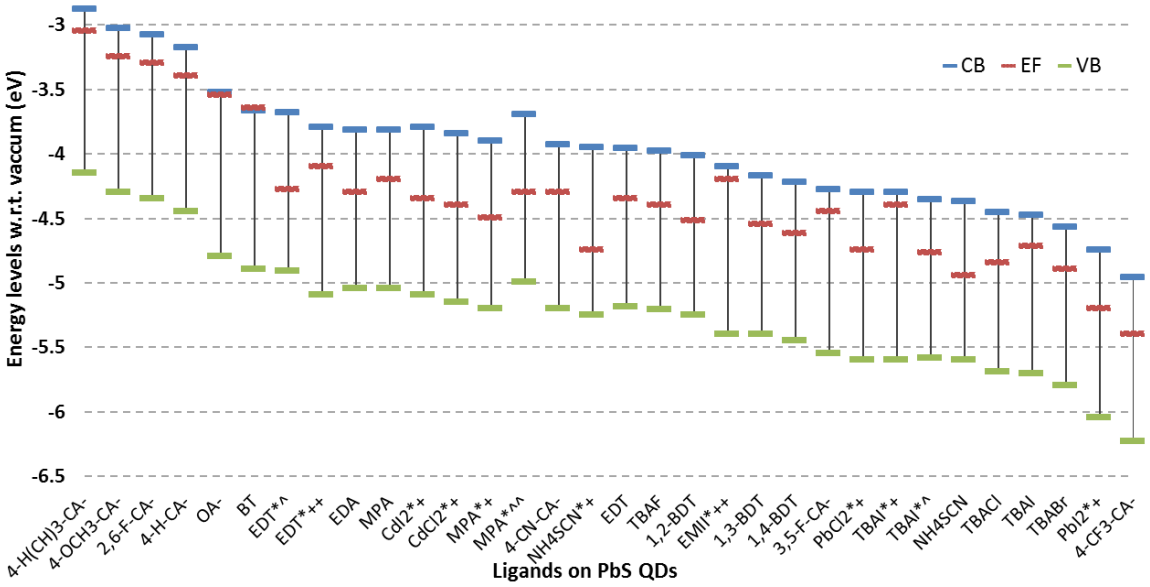

Figure 5. A compilation of the effect of 29 different QD surface passivating ligand species on the energy levels of PbS QDs with a bandgap of ≈1.3 eV from literature [144,145,174,176–178]. It is observed that more electronegative species push the energy levels deeper due to their higher affinity to hold electrons inside the QD by establishing a strong electric field around the QD. Samples prepared under ambient conditions are represented by the superscript "*" while other superscripts like "+" [144], "^" [174], "++" [178], "^^" [176] differentiate the energy level values obtained in different literature cited for similar ligand treatments. The red, black and green lines represent the CB minimum, Fermi level and the VB minimum respectively. Details are available in the Supplementary Materials.

In 2010, Abraham et al. [172] developed a planar depleted heterojunction configuration for QDSCs after significant work starting with QDs blended with conductive polymers [179,180]. These devices were the first to break the 5% PCE mark and hence formed a basis for future research. In such a configuration, the heterojunction is formed between the light absorbing QD layer and a wide bandgap n-doped electrode like TiO_2 or zinc oxide (ZnO) which acts as an electron accepting and hole blocking layer as seen in Figure 4. The holes are collected at the back contact using a deep work function metal like gold (Au) while the electrons are collected at the top contact which is typically a transparent conductive oxide (TCO) like ITO or fluorine-doped tin oxide (FTO). The presence of states inside the bandgap in real QDs leads to small minority carrier diffusion lengths in the QD film. This leads to significant difficulty in extracting minority charge carriers formed on photoexcitation in such planar devices, which is tackled by driving the minority carrier transport by the electric field formed by the space charge region (depletion width) at the heterojunction. The QD absorber layer thickness in such a case is limited to the sum of the depletion width and diffusion length, which ensures that the charge carrier formed farthest away from the heterojunction can diffuse until it reaches the space charge region and then be transported to the other side of the junction by the electric field. In the following years, this depleted heterojunction QDSC configuration has undergone several modifications leading to solar cell PCE exceeding 10% [181–197]. The following paragraphs will detail the development of high-efficiency heterojunction QDSCs.

In the beginning of the depleted heterojunction QDSC development, short, organic ligands like 1,2-ethanedithiol (EDT) and 3-mercaptopropionic acid were exchanged with the insulating oleate ligands due to their ability to p-dope the absorber layer and allow better electronic coupling between neighboring QDs in films. While EDT was predominantly used to make such devices, Jeong et al. [128] showed that MPA ligand-exchanged PbS QD films performed much better than EDT

ligand-exchanged films due to its ability to passivate the QD surface better and pack QDs closer than with EDT ligands leading to higher carrier mobilities. Following the rise in usage of MPA, in 2014, Chuang et al. [174] developed an approach that involved engineering the band alignment of the PbS QDs based on the interaction of QD films with two different ligands. The PbS QDSCs fabricated with the method from Chuang et al. showed a PCE of 8.55% that thereafter became the norm in depleted heterojunction QDSCs. In this approach, each deposited layer of the oleate-capped PbS QD film in the entire stack was ligand-exchanged with tetrabutylammonium iodide (TBAI) except the final two layers that were instead ligand-exchanged with EDT—similar to what Semonin et al. [79] observed using EDT and hydrazine in order to observe carrier multiplication in EQE measurements. The deeper energy levels of iodide-capped PbS QD films align with the shallower energy levels of the EDT-capped PbS QD films to create an energetic barrier for electrons. With this alignment, electrons flow from the EDT-capped layers to the iodide-capped layers resulting in favorable band bending forming an electron blocking layer to prevent electron recombination at the rear metal contact. Using the same configuration, other research groups have obtained similar results using other ligand combinations with functionalities like PbI_2 and MPA [144], 1-ethyl-3-methylimidazolium iodide (EMII) and EDT [178,187,188] and 1-propyl-2,3-dimethyl-imidazolium iodide (PDMII) and 1,3-propane dithiol (PDT) [183,184]. Using PbI_2 and mercaptopropionic (MPA) ligands, Crisp et al. [144] reported solar cells with thickness optimized at over 500 nm, almost double the thickness of other record-setting devices, due to favorable band alignments between the layers on the cell and improved surface passivation of PbI_2 over other halide treatments. The reproducibility and stability of such treatments then allowed for further optimization of other components in the device structure and fabrication procedures.

The primary area of improvement that researchers have focused on has been the improvement of the diffusion length of minority carriers in PbS QDs. While solid-state ligand exchange techniques have been shown to effectively replace the oleate ligands attached to the as-prepared QD surface, it does not fully protect the QD surface and a certain percentage of trap states remain [198,199]—some of which could arise from fusing of QDs during the ligand exchange forming dimers that naturally have lower energy levels in the bandgap of the other QDs [181,200]. As a result, solution phase passivation techniques were adopted. First, a post-synthesis treatment to improve the surface passivation with metal halides was used [201]. It was observed that this process replaced some oleate ligands while retaining enough to maintain the stability of the QDs in the non-polar solvent (usually octane). Due to their small size, halides have shown very good passivating capabilities and have been extensively used in solution phase passivation techniques. Cadmium chloride—$CdCl_2$ (provided Cd^{2+} and halide passivation of the S^{2-} and Pb^{2+} vacancies) [201], TBAI [202,203], molecular iodine (I_2) [181], methyl ammonium iodide (MAI, a milder I source) [182] and Trimethylsilyl chloride (TMS-Cl in n-hexylamine and n-octylamine) [137] are a few examples of the ligands that have been used effectively in solution phase ligand passivation of PbS QDSCs. The TMS-Cl passivation of QDs has also resulted in a record diffusion length of ≈230 nm arising from the partial fusion of neighboring QDs. Additionally, it was observed that of these techniques, MAI's ability to controllably strip oleate ligands and subsequently passivate the QD surface well with I_2 has led to QDSCs with PCEs as high as 10.6% [182] and that QDSC devices made using I_2 ligand passivation were found to be the most air-stable [203].

While all the above devices involved developing the QD absorber by a layer-by-layer (LbL) deposition method coupled with consecutive solid-state ligand exchange and rinsing steps, a single step deposition method involving complete ligand exchange through solution-phase ligand exchange was explored to simplify device fabrication. One of the major hurdles in such a single step method was finding the best solvent that could maintain the stability of the QDs capped with shorter ligands in solution and at the same time evaporate in such a way that leads to smooth, uniform, and crack-free films. Sargent and co-workers [204], at a similar time as the Kovalenko group [205,206], developed a strategy involving a solution-phase exchange of the oleate ligands from the PbS QDs in octane with iodide ligands present in a polar solvent like *N*,*N*-dimethylformamide (DMF). The immiscibility of the two solvents allows the easy separation of the two phases formed and the I^--capped QDs dissolved in

DMF are then washed and dispersed in n-butylamine with a very high concentration (≈200 mg/mL). This CQD ink is then deposited in a single step (as opposed to LbL deposition) to obtain QD films of the required thickness and uniformity. While MAI, sodium iodide (NaI) [204] and PbI_2 [207] have been used as iodine sources, a mixture of PbI_2/$PbBr_2$/ammonium acetate (NH_4Ac) has shown the best results leading to PbS QDSCs with PCEs of 11.28% [193] and 11.6% [192].

In addition to new passivation techniques to improve the diffusion length in PbS QD films, researchers have also worked on increasing the width of the depletion region in the absorber layer to improve drift-based carrier transport. In PbS QDSCs with a bilayer configuration like the one developed by Chuang et al. [174], the existence of 2 junctions, the n+/n heterojunction between ZnO (or TiO_2) and the n/p quantum junction between I^- capped and EDT capped PbS (also called the hole transport layer, HTL) makes it interesting to optimize the device architecture. Techniques like substitutional doping of the ZnO layer by incorporating indium [191] or magnesium [186,190] into the ZnO lattice in sol-gel-based ZnO, the chloride passivation of oxygen vacancies in ZnO NC films by treating the film with sodium chloride (NaCl) [192] and the soaking of ZnO NC films in ultraviolet (UV) light to release gaseous molecules possibly adsorbed onto the ZnO NC surface [208] have demonstrated that increasing the n-doping in the n+ layer has indeed resulted in an improved performance of PbS QDSCs. Analogously, increased p-type doping of the HTL via molecular doping [18] and sodium hydrosulphide (NaHS) treatment [209] has also shown to increase the depletion width in the absorber layer in addition to improving band bending at the interface during the maximum power point condition leading to high fill factors (FF) and high PCE solar cells. Introducing extra electron transport layers (ETLs) and HTLs [196,210–213] at these interfaces have also been reported to improve device performance. ETLs are chosen such that they passivate the surface defects present in the metal oxide layer and also promote favorable band bending at the interface between the metal oxide layer and the n type QD films that improves the built-in and open circuit voltage. These ETLs can be self-assembled monolayers (SAMs) formed by treating the metal oxide layer with organic solutions like tetrahydrofuran [184] and aminobenzoic acid [197] or other intermediate buffer layers made of materials like carbon QDs [212], CdSe QDs [214], mixed nanocrystals [188], magnesium-doped ZnO [215] or other organic buffers [216] that have given rise to devices with PCEs >9%. While all these ETLs are used in conjunction with a metal oxide layer, recently, CdS has also been successfully used as an n-type electrode instead of a metal oxide to make a heterojunction QDSC with a PCE of 8% [217].

Despite the high performance of heterojunction solar cell, there are some inherent disadvantages associated with such a configuration. The misalignment of bands at the junction could potentially lead to a loss in open circuit voltage and improper charge injection into the n-type window layer for QD films with a smaller bandgap [218]. Thus, the ideal QDSC configuration would be to have a specific bandgap tuned PbS QD film with p- and n-type doping on opposite side of the p-n junction that has the entire p-n junction absorbing light to produce photo-generated carriers. Such quantum junction solar cells (QJSCs) have also been developed with p-type doping being achieved through physical deposition of the oleate capped PbS layer in air followed by tetramethylammonium hydroxide (TMAOH) treatment and air annealing. On top of the p-type layer, n-type doping through iodide treatment inside an N_2 filled glovebox [181,218] completes the p-n junction. Further modifications through the addition of an n+ layer in between the iodide treated film and the metal contact [219] and replacing the iodide ligand-exchanged n-type layer with an n-type CQD ink as discussed earlier have resulted in performance enhancement leading to PCE as high as 8% [203]. Similar doping strategies using S^{2-} have shown promise creating n-type HgS QDs for photodetectors [220].

Though PbS has been the most explored QD material in QDSCs, theoretically, PbSe shows better promise to overcome the Shockley-Queisser limit for solar cell devices. PbSe's larger Bohr exciton radius improves quantum confinement of charge carriers in the QDs which in turn increases the probability of carrier multiplication as evidenced by the work of Semonin et al. [79] and Davis et al. [80]. Similar to PbS QDSC devices, PbSe QDSC devices were first fabricated in Schottky junction configuration [5,167,221] following which the heterojunction configuration was adopted. In this configuration, devices with PCE

greater than 5% have been achieved through a combination of effective PbSe QD synthesis protocols and different solid-state ligand exchange treatments. Zhang et al. [222] and Kim et al. [223] devised cation exchange reactions to synthesize PbSe from CdSe and ZnSe, respectively, which resulted in QDSC devices with PCE greater than 5% and superior air-stability due to possible surface passivation by a metal and halide ions. While the insulating oleate ligands in as-prepared PbSe QD films were replaced with shorter and more conductive EDT in early PbSe QDSC devices, Zhang et al.'s [224] work showed that solid state ligand exchange with TBAI ligands provided the best results by comparing the effect of TBAI, EDT, MPA and cetyltrimethylammonium bromide (CTAB) on device performance. By adopting techniques used in PbS QDSCs, the performance of PbSe QDSCs has also improved in recent times. Kim et al. [223] fabricated air-stable devices with a PCE ≈6% using the bi-layer configuration, while Zhang et al. [225] added an additional $CsPbBr_3$ HTL in between the MPA exchanged layer and the back contact to improve hole transfer and consequently the device FF and PCE. Using a PbSe CQD ink with PbI_2 surface passivation similar to that made by Sargent and co-workers [207], Zhang et al. [226] were able to fabricate high-efficiency QDSC devices through a single step deposition method as opposed to the LbL deposition process through spin/dip coating. The Huang group's unique halide passivation technique of the PbSe QDs using Cs-based perovskite NCs has helped achieve a PCE of 8.2% [227] which currently is the world record efficiency for PbSe QDSC devices.

Figure 6 plots the PCE and V_{OC} of all PbS and PbSe QDSCs as a function of the QD bandgap that we could find in the literature. Figure 6a shows the majority of the devices use QDs around 1.3 eV (the theoretical optimum bandgap for a single junction solar cell). However, one of the biggest strengths of QDs is their tunable bandgap, which could be used more to complement other existing technologies. For instance, using QDs in combination with commercial Si or CdTe cells could boost their efficiency in a tandem configuration [95–98,228,229].

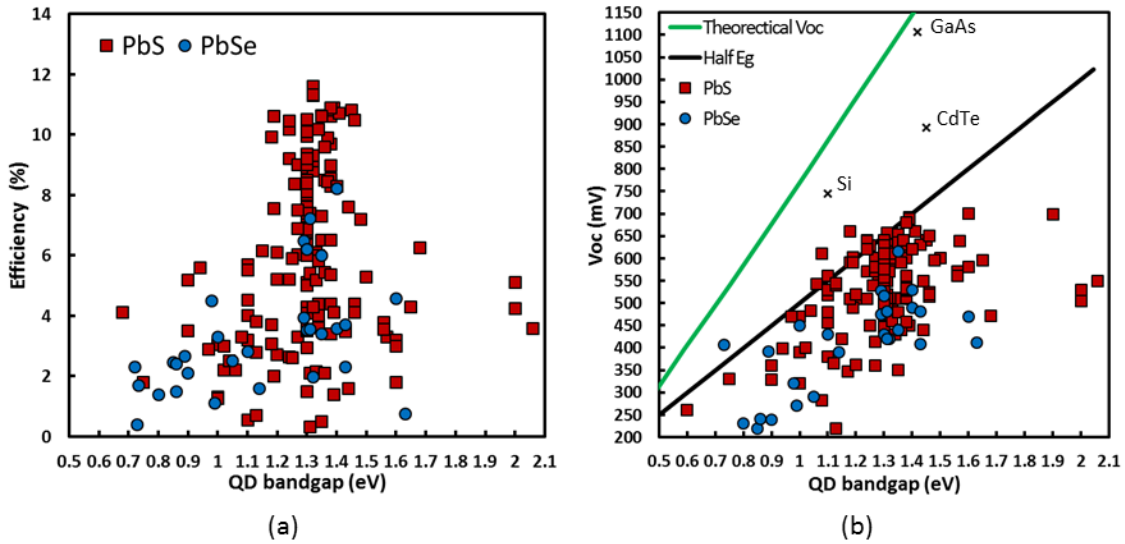

Figure 6. (**a**) The power conversion efficiency of PbS and PbSe QDSCs as a function of QD bandgap reported in the literature (data given in the Supplementary Materials). (**b**) The open circuit voltage (V_{OC}) of all PbS and PbSe QD solar cells in the literature as a function of band gap with lines showing the theoretical maximum V_{OC} (green) and 1/2 the bandgap (black) highlighting the deficit QD solar cells have compared to Si, GaAs, and CdTe record efficiency solar cells shown with X symbols (data in Supplementary Materials).

While most of the high-efficiency QDSC configurations have used a deep work function metal like Au as the rear metal contact, Gao et al.'s [230] work has shown the formation of a Schottky barrier for holes at the rear PbS/metal leading to current saturation at higher forward applied voltages. This motivated the use of different combinations of rear metal contacts to induce

a favorable band bending for both electrons and holes. While Au is predominantly used for this purpose, a combination of stepwise decreasing work function metals like Au/Ag or MoO_x/Au/Ag or AZO/Ag (AZO is aluminum-doped zinc oxide) has also been adopted by a few research groups. Other than this, a few others have also adopted the use of inorganic materials like molybdenum oxide (MoO_x) [231,232], or other organic materials like poly(3-hexylthiophene-2,5-diyl) (P3HT) [233], 2,2′,7,7′-tetrakis(*N*,*N*-di-p-methoxyphenylamine)-9,9′-spirobifluorene (Spiro-OMeTAD) and bis-triphenylamine (BTPA-4) [211] as hole selective layers to solve this problem. Despite favorable results with MoO_x under inert conditions, Chuang et al. [174] showed that the devices with MoO_x lacked air-stability due to MoO_x's possible oxidation that results in the lowering of its work function and thus unfavorable band bending at the interface. While different configurations seemed to have worked for different devices, a systematic study of any possible device performance enhancement by optimizing this interface has not yet been studied.

Other record-setting PbS devices include those developed by Choi et al. [192] with a PCE of 11.6% based on a CQD ink and Lu et al. [195] with a PCE of 11.21% based on solid-state ligand exchange. Though in recent years, perovskite-based QDs have also been fabricated based on cesium lead iodide ($CsPbI_3$) [234,235] one of which developed at the National Renewable Energy Laboratories (NREL) currently holds the world record for QD-based solar cells with PCE of 13.23% [236].

One of the main limitations of current QDSCs is their V_{OC} deficit, i.e., the difference between the bandgap energy and the open circuit voltage [199,237,238]. There are several factors that could contribute to loss: Urbach or energy tails [239,240], recombination/trap states [170,237,241], large dark current [242], and insufficient heterojunction characteristics [237]. Figure 6b shows that regardless of device configuration, bandgap, or research group (with the exception of 2 devices) the practical limit for the V_{OC} is ~1/2 the bandgap (black line). The disorder in the energy landscape caused by film formation (e.g., QD necking, random packing) that leads to energy tailing and mid-gap states could be mitigated by further improvements in film formation of superlattices (long-range ordering of QDs) [243–250].

In summary, we described the processes that occur when a QD absorbs a photon and how these energy flow pathways influence quantum dot solar cells. Furthermore, we present a description of the history of PbS and PbSe QDs used in solar cells and compile device results from the literature to present a complete picture of the state-of-the-art in QDSC technology. We thus propose further work using the newest fundamental breakthroughs in synthesis, ligation, device architecture, and QD film assembly to continue to improve the PCE.

Supplementary Materials: The following are available online at http://www.mdpi.com/2076-3417/8/10/1867/s1, tabulated data of QD energy levels vs ligand, performance parameters of all PbS, PbSe, PbTe, and certain QD tandem solar cells used in Figures 5 and 6.

Author Contributions: All authors aided in writing and preparing the manuscript.

Funding: A.J.H. and R.W.C. received support from STW (project No. 13903, Stable and Non-Toxic Nanocrystal Solar Cells). A.J.H. further acknowledges support from the European Research Council Horizon 2020 ERC Grant Agreement No. 678004 (Doping on Demand).

Acknowledgments: The authors thank Ashely Marshall for aid in collating the Supplementary Materials spreadsheet.

Conflicts of Interest: The authors declare no conflict of interest.

References

1. Brus, L. Electronic wave functions in semiconductor clusters: Experiment and theory. *J. Phys. Chem.* **1986**, *90*, 2555–2560. [CrossRef]
2. Efros, A.L.; Rosen, M. Quantum size level structure of narrow-gap semiconductor nanocrystals: Effect of band coupling. *Phys. Rev. B* **1998**, *58*, 7120–7135. [CrossRef]
3. Aabhash, S.; Munkhbayar, B.; Antonio, T.; Sheng, D.; Zhang, Q.S. Recent advance in near-infrared active lead chalcogenide quantum dots: Preparation, post-synthesis ligand exchange and applications in solar cells. *Angew. Chem. Int. Ed.* **2018**. [CrossRef]

4. Lim, J.; Bae, W.K.; Kwak, J.; Lee, S.; Lee, C.; Char, K. Perspective on synthesis, device structures, and printing processes for quantum dot displays. *Opt. Mater. Express* **2012**, *2*, 594–628. [CrossRef]
5. Murray, C.B.; Kagan, C.R.; Bawendi, M.G. Synthesis and characterization of monodisperse nanocrystals and close-packed nanocrystal assemblies. *Annu. Rev. Mater. Sci.* **2000**, *30*, 545–610. [CrossRef]
6. Kershaw, S.V.; Susha, A.S.; Rogach, A.L. Narrow bandgap colloidal metal chalcogenide quantum dots: Synthetic methods, heterostructures, assemblies, electronic and infrared optical properties. *Chem. Soc. Rev.* **2013**, *42*, 3033–3087. [CrossRef] [PubMed]
7. Owen, J.; Brus, L. Chemical synthesis and luminescence applications of colloidal semiconductor quantum dots. *J. Am. Chem. Soc.* **2017**, *139*, 10939–10943. [CrossRef] [PubMed]
8. van Embden, J.; Chesman, A.S.R.; Jasieniak, J.J. The heat-up synthesis of colloidal nanocrystals. *Chem. Mater.* **2015**, *27*, 2246–2285. [CrossRef]
9. Goubet, N.; Jagtap, A.; Livache, C.; Martinez, B.; Portalès, H.; Xu, X.Z.; Lobo, R.P.S.M.; Dubertret, B.; Lhuillier, E. Terahertz hgte nanocrystals: Beyond confinement. *J. Am. Chem. Soc.* **2018**, *140*, 5033–5036. [CrossRef] [PubMed]
10. LaMer, V.K.; Dinegar, R.H. Theory, production and mechanism of formation of monodispersed hydrosols. *J. Am. Chem. Soc.* **1950**, *72*, 4847–4854. [CrossRef]
11. Sugimoto, T.; Shiba, F.; Sekiguchi, T.; Itoh, H. Spontaneous nucleation of monodisperse silver halide particles from homogeneous gelatin solution i: Silver chloride. *Colloids Surf. A Physicochem. Eng. Asp.* **2000**, *164*, 183–203. [CrossRef]
12. Liu, H.; Owen, J.S.; Alivisatos, A.P. Mechanistic study of precursor evolution in colloidal group II–VI semiconductor nanocrystal synthesis. *J. Am. Chem. Soc.* **2007**, *129*, 305–312. [CrossRef] [PubMed]
13. Clark, M.D.; Kumar, S.K.; Owen, J.S.; Chan, E.M. Focusing nanocrystal size distributions via production control. *Nano Lett.* **2011**, *11*, 1976–1980. [CrossRef] [PubMed]
14. Hendricks, M.P.; Campos, M.P.; Cleveland, G.T.; Jen-La Plante, I.; Owen, J.S. A tunable library of substituted thiourea precursors to metal sulfide nanocrystals. *Science* **2015**, *348*, 1226–1230. [CrossRef] [PubMed]
15. Campos, M.P.; Hendricks, M.P.; Beecher, A.N.; Walravens, W.; Swain, R.A.; Cleveland, G.T.; Hens, Z.; Sfeir, M.Y.; Owen, J.S. A library of selenourea precursors to PbSe nanocrystals with size distributions near the homogeneous limit. *J. Am. Chem. Soc.* **2017**, *139*, 2296–2305. [CrossRef] [PubMed]
16. Hamachi, L.S.; Jen-La Plante, I.; Coryell, A.C.; De Roo, J.; Owen, J.S. Kinetic control over CdS nanocrystal nucleation using a library of thiocarbonates, thiocarbamates, and thioureas. *Chem. Mater.* **2017**, *29*, 8711–8719. [CrossRef]
17. Yarema, M.; Caputo, R.; Kovalenko, M.V. Precision synthesis of colloidal inorganic nanocrystals using metal and metalloid amides. *Nanoscale* **2013**, *5*, 8398–8410. [CrossRef] [PubMed]
18. Tessier, M.D.; De Nolf, K.; Dupont, D.; Sinnaeve, D.; De Roo, J.; Hens, Z. Aminophosphines: A double role in the synthesis of colloidal indium phosphide quantum dots. *J. Am. Chem. Soc.* **2016**, *138*, 5923–5929. [CrossRef] [PubMed]
19. Crisp, R.W.; Grimaldi, G.; De Trizio, L.; Evers, W.; Kirkwood, N.; Kinge, S.; Manna, L.; Siebbeles, L.; Houtepen, A.J. Selective antimony reduction initiating the nucleation and growth of insb quantum dots. *Nanoscale* **2018**, *10*, 11110–11116. [CrossRef] [PubMed]
20. Zhang, J.; Gao, J.; Miller, E.M.; Luther, J.M.; Beard, M.C. Diffusion-controlled synthesis of PbS and PbSe quantum dots with in situ halide passivation for quantum dot solar cells. *ACS Nano* **2013**, *8*, 614–622. [CrossRef] [PubMed]
21. Zhang, J.; Crisp, R.W.; Gao, J.; Kroupa, D.M.; Beard, M.C.; Luther, J.M. Synthetic conditions for high-accuracy size control of PbS quantum dots. *J. Phys. Chem. Lett.* **2015**, *6*, 1830–1833. [CrossRef] [PubMed]
22. Steckel, J.S.; Yen, B.K.H.; Oertel, D.C.; Bawendi, M.G. On the mechanism of lead chalcogenide nanocrystal formation. *J. Am. Chem. Soc.* **2006**, *128*, 13032–13033. [CrossRef] [PubMed]
23. Keuleyan, S.; Lhuillier, E.; Guyot-Sionnest, P. Synthesis of colloidal hgte quantum dots for narrow mid-IR emission and detection. *J. Am. Chem. Soc.* **2011**, *133*, 16422–16424. [CrossRef] [PubMed]
24. Heyes, C.D.; Kobitski, A.Y.; Breus, V.V.; Nienhaus, G.U. Effect of the shell on the blinking statistics of core-shell quantum dots: A single-particle fluorescence study. *Phys. Rev. B* **2007**, *75*, 125431. [CrossRef]
25. Tomaselli, M.; Yarger, J.L.; Bruchez, M., Jr.; Havlin, R.H.; deGraw, D.; Pines, A.; Alivisatos, A.P. Nmr study of inp quantum dots: Surface structure and size effects. *J. Chem. Phys.* **1999**, *110*, 8861–8864. [CrossRef]

26. Hines, D.A.; Kamat, P.V. Recent advances in quantum dot surface chemistry. *ACS Appl. Mater. Interfaces* **2014**, *6*, 3041–3057. [CrossRef] [PubMed]
27. Kagan, C.R.; Murray, C.B. Charge transport in strongly coupled quantum dot solids. *Nat. Nanotechnol.* **2015**, *10*, 1013–1026. [CrossRef] [PubMed]
28. Grim, J.Q.; Manna, L.; Moreels, I. A sustainable future for photonic colloidal nanocrystals. *Chem. Soc. Rev.* **2015**, *44*, 5897–5914. [CrossRef] [PubMed]
29. De Trizio, L.; Manna, L. Forging colloidal nanostructures via cation exchange reactions. *Chem. Rev.* **2016**, *116*, 10852–10887. [CrossRef] [PubMed]
30. Talapin, D.V.; Lee, J.-S.; Kovalenko, M.V.; Shevchenko, E.V. Prospects of colloidal nanocrystals for electronic and optoelectronic applications. *Chem. Rev.* **2009**, *110*, 389–458. [CrossRef] [PubMed]
31. Nath, G.H.; Sourav, M.; Jayanta, D. Correlating charge carrier dynamics with efficiency in quantum dot solar cells: Can excitonics lead to highly efficient devices? *Chem. A Eur. J.* **2018**. [CrossRef]
32. Huxter, V.M.; Scholes, G. Photophysics of colloidal semiconductor nanocrystals: A review. *NANOP* **2009**, *3*, 032504. [CrossRef]
33. Guyot-Sionnest, P. Electrical transport in colloidal quantum dot films. *J. Phys. Chem. Lett.* **2012**, *3*, 1169–1175. [CrossRef] [PubMed]
34. Stolle, C.J.; Harvey, T.B.; Korgel, B.A. Nanocrystal photovoltaics: A review of recent progress. *Curr. Opin. Chem. Eng.* **2013**, *2*, 160–167. [CrossRef]
35. Albero, J.; Clifford, J.N.; Palomares, E. Quantum dot based molecular solar cells. *Coord. Chem. Rev.* **2014**, *263–264*, 53–64. [CrossRef]
36. Carey, G.H.; Abdelhady, A.L.; Ning, Z.; Thon, S.M.; Bakr, O.M.; Sargent, E.H. Colloidal quantum dot solar cells. *Chem. Rev.* **2015**, *115*, 12732–12763. [CrossRef] [PubMed]
37. Kim, M.R.; Ma, D. Quantum-dot-based solar cells: Recent advances, strategies, and challenges. *J. Phys. Chem. Lett.* **2015**, *6*, 85–99. [CrossRef] [PubMed]
38. Chistyakov, A.A.; Zvaigzne, M.A.; Nikitenko, V.R.; Tameev, A.R.; Martynov, I.L.; Prezhdo, O.V. Optoelectronic properties of semiconductor quantum dot solids for photovoltaic applications. *J. Phys. Chem. Lett.* **2017**, *8*, 4129–4139. [CrossRef] [PubMed]
39. Liu, Z.; Yuan, J.; Hawks, S.A.; Shi, G.; Lee, S.-T.; Ma, W. Photovoltaic devices based on colloidal PbX quantum dots: Progress and prospects. *Solar RRL* **2017**, 1600021. [CrossRef]
40. Song, J.H.; Jeong, S. Colloidal quantum dot based solar cells: From materials to devices. *Nano Converg.* **2017**, *4*, 21. [CrossRef] [PubMed]
41. Singhal, P.; Ghosh, H.N. Hot charge carrier extraction from semiconductor quantum dots. *J. Phys. Chem. C* **2018**, *122*, 17586–17600. [CrossRef]
42. Leatherdale, C.A.; Woo, W.K.; Mikulec, F.V.; Bawendi, M.G. On the absorption cross section of CdSe nanocrystal quantum dots. *J. Phys. Chem. B* **2002**, *106*, 7619–7622. [CrossRef]
43. Ricard, D.; Ghanassi, M.; Schanne-Klein, M.C. Dielectric confinement and the linear and nonlinear optical properties of semiconductor-doped glasses. *Opt. Commun.* **1994**, *108*, 311–318. [CrossRef]
44. Luther, J.M.; Jain, P.K.; Ewers, T.; Alivisatos, A.P. Localized surface plasmon resonances arising from free carriers in doped quantum dots. *Nat. Mater.* **2011**, *10*, 361. [CrossRef] [PubMed]
45. Paz-Soldan, D.; Lee, A.; Thon, S.M.; Adachi, M.M.; Dong, H.; Maraghechi, P.; Yuan, M.; Labelle, A.J.; Hoogland, S.; Liu, K.; et al. Jointly tuned plasmonic-excitonic photovoltaics using nanoshells. *Nano Lett.* **2013**, *13*, 1502–1508. [CrossRef] [PubMed]
46. Kawawaki, T.; Wang, H.; Kubo, T.; Saito, K.; Nakazaki, J.; Segawa, H.; Tatsuma, T. Efficiency enhancement of PbS quantum dot/ZnO nanowire bulk-heterojunction solar cells by plasmonic silver nanocubes. *ACS Nano* **2015**, *9*, 4165–4172. [CrossRef] [PubMed]
47. Baek, S.-W.; Song, J.H.; Choi, W.; Song, H.; Jeong, S.; Lee, J.-Y. A resonance-shifting hybrid n-type layer for boosting near-infrared response in highly efficient colloidal quantum dots solar cells. *Adv. Mater.* **2015**, *27*, 8102–8108. [CrossRef] [PubMed]
48. Chen, S.; Wang, Y.J.; Liu, Q.; Shi, G.; Liu, Z.; Lu, K.; Han, L.; Ling, X.; Zhang, H.; Cheng, S.; et al. Broadband enhancement of PbS quantum dot solar cells by the synergistic effect of plasmonic gold nanobipyramids and nanospheres. *Adv. Energy Mater.* **2018**, *8*, 1–9. [CrossRef]

49. Lhuillier, E.; Scarafagio, M.; Hease, P.; Nadal, B.; Aubin, H.; Xu, X.Z.; Lequeux, N.; Patriarche, G.; Ithurria, S.; Dubertret, B. Infrared photodetection based on colloidal quantum-dot films with high mobility and optical absorption up to thz. *Nano Lett.* **2016**, *16*, 1282–1286. [CrossRef] [PubMed]
50. Keuleyan, S.E.; Guyot-Sionnest, P.; Delerue, C.; Allan, G. Mercury telluride colloidal quantum dots: Electronic structure, size-dependent spectra, and photocurrent detection up to 12 µm. *ACS Nano* **2014**, *8*, 8676–8682. [CrossRef] [PubMed]
51. Chen, M.; Shao, L.; Kershaw, S.V.; Yu, H.; Wang, J.; Rogach, A.L.; Zhao, N. Photocurrent enhancement of hgte quantum dot photodiodes by plasmonic gold nanorod structures. *ACS Nano* **2014**, *8*, 8208–8216. [CrossRef] [PubMed]
52. Tang, X.; Wu, G.F.; Lai, K.W.C. Plasmon resonance enhanced colloidal HgSe quantum dot filterless narrowband photodetectors for mid-wave infrared. *J. Mater. Chem. C* **2017**, *5*, 362–369. [CrossRef]
53. Tang, X.; Ackerman, M.M.; Guyot-Sionnest, P. Thermal imaging with plasmon resonance enhanced hgte colloidal quantum dot photovoltaic devices. *ACS Nano* **2018**, *12*, 7362–7370. [CrossRef] [PubMed]
54. Jean, J.; Chang, S.; Brown, P.R.; Cheng, J.J.; Rekemeyer, P.H.; Bawendi, M.G.; Gradečak, S.; Bulović, V. ZnO nanowire arrays for enhanced photocurrent in PbS quantum dot solar cells. *Adv. Mater.* **2013**, *25*, 2790–2796. [CrossRef] [PubMed]
55. Nozik, A.J.; Beard, M.C.; Luther, J.M.; Law, M.; Ellingson, R.J.; Johnson, J.C. Semiconductor quantum dots and quantum dot arrays and applications of multiple exciton generation to third-generation photovoltaic solar cells. *Chem. Rev.* **2010**, *110*, 6873–6890. [CrossRef] [PubMed]
56. Ackerman, M.M.; Tang, X.; Guyot-Sionnest, P. Fast and sensitive colloidal quantum dot mid-wave infrared photodetectors. *ACS Nano* **2018**, *12*, 7264–7271. [CrossRef] [PubMed]
57. Law, M.; Beard, M.C.; Choi, S.; Luther, J.M.; Hanna, M.C.; Nozik, A.J. Determining the internal quantum efficiency of PbSe nanocrystal solar cells with the aid of an optical model. *Nano Lett.* **2008**, *8*, 3904–3910. [CrossRef] [PubMed]
58. Adachi, M.M.; Labelle, A.J.; Thon, S.M.; Lan, X.; Hoogland, S.; Sargent, E.H. Broadband solar absorption enhancement via periodic nanostructuring of electrodes. *Sci. Rep.* **2013**, *3*, 2928. [CrossRef] [PubMed]
59. Mihi, A.; Beck, F.J.; Lasanta, T.; Rath, A.K.; Konstantatos, G. Imprinted electrodes for enhanced light trapping in solution processed solar cells. *Adv. Mater.* **2014**, *26*, 443–448. [CrossRef] [PubMed]
60. Labelle, A.J.; Thon, S.M.; Kim, J.Y.; Lan, X.; Zhitomirsky, D.; Kemp, K.W.; Sargent, E.H. Conformal fabrication of colloidal quantum dot solids for optically enhanced photovoltaics. *ACS Nano* **2015**, *9*, 5447–5453. [CrossRef] [PubMed]
61. Kim, Y.; Bicanic, K.; Tan, H.; Ouellette, O.; Sutherland, B.R.; García de Arquer, F.P.; Jo, J.W.; Liu, M.; Sun, B.; Liu, M.; et al. Nanoimprint-transfer-patterned solids enhance light absorption in colloidal quantum dot solar cells. *Nano Lett.* **2017**, *17*, 2349–2353. [CrossRef] [PubMed]
62. Labelle, A.J.; Thon, S.M.; Masala, S.; Adachi, M.M.; Dong, H.; Farahani, M.; Ip, A.H.; Fratalocchi, A.; Sargent, E.H. Colloidal quantum dot solar cells exploiting hierarchical structuring. *Nano Lett.* **2015**, *15*, 1101–1108. [CrossRef] [PubMed]
63. Hens, Z.; Moreels, I. Light absorption by colloidal semiconductor quantum dots. *J. Mater. Chem.* **2012**, *22*, 10406–10415. [CrossRef]
64. Giansante, C.; Infante, I.; Fabiano, E.; Grisorio, R.; Suranna, G.P.; Gigli, G. "Darker-than-black" PbS quantum dots: Enhancing optical absorption of colloidal semiconductor nanocrystals via short conjugated ligands. *J. Am. Chem. Soc.* **2015**, *137*, 1875–1886. [CrossRef] [PubMed]
65. Boles, M.A.; Ling, D.; Hyeon, T.; Talapin, D.V. The surface science of nanocrystals. *Nat. Mater.* **2016**, *15*, 141–153. [CrossRef] [PubMed]
66. Kroupa, D.M.; Arias, D.H.; Blackburn, J.L.; Carroll, G.M.; Granger, D.B.; Anthony, J.E.; Beard, M.C.; Johnson, J.C. Control of energy flow dynamics between tetracene ligands and PbS quantum dots by size tuning and ligand coverage. *Nano Lett.* **2018**, *18*, 865–873. [CrossRef] [PubMed]
67. Kroupa, D.; Vörös, M.; Brawand, N.P.; Bronstein, N.D.; McNichols, B.W.; Castaneda, C.V.; Nozik, A.J.; Sellinger, A.; Galli, G.; Beard, M.C. Optical absorbance enhancement in PbS qd/cinnamate ligand complexes. *J. Phys. Chem. Lett.* **2018**, *9*, 3425–3433. [CrossRef] [PubMed]
68. Geiregat, P.; Justo, Y.; Abe, S.; Flamee, S.; Hens, Z. Giant and broad-band absorption enhancement in colloidal quantum dot mono layers through dipolar coupling. *ACS Nano* **2013**, *7*, 987–993. [CrossRef] [PubMed]

69. Sandeep, C.S.S.; Azpiroz, J.M.; Evers, W.H.; Boehme, S.C.; Moreels, I.; Kinge, S.; Siebbeles, L.D.A.; Infante, I.; Houtepen, A.J. Epitaxially connected PbSe quantum-dot films: Controlled neck formation and optoelectronic properties. *ACS Nano* **2014**, *8*, 11499–11511. [CrossRef] [PubMed]
70. Scheele, M.; Brutting, W.; Schreiber, F. Coupled organic-inorganic nanostructures (coin). *PCCP* **2015**, *17*, 97–111. [CrossRef] [PubMed]
71. André, A.; Theurer, C.; Lauth, J.; Maiti, S.; Hodas, M.; Samadi Khoshkhoo, M.; Kinge, S.; Meixner, A.J.; Schreiber, F.; Siebbeles, L.D.A.; et al. Structure, transport and photoconductance of PbS quantum dot monolayers functionalized with a copper phthalocyanine derivative. *Chem. Commun.* **2017**, *53*, 1700–1703. [CrossRef] [PubMed]
72. Tang, X.; Wu, G.F.; Lai, K.W.C. Twisted graphene-assisted photocarrier transfer from HgSe colloidal quantum dots into silicon with enhanced collection and transport efficiency. *Appl. Phys. Lett.* **2017**, *110*, 241104. [CrossRef]
73. Lauth, J.; Grimaldi, G.; Kinge, S.; Houtepen, A.J.; Siebbeles, L.D.A.; Scheele, M. Ultrafast charge transfer and upconversion in zinc β-tetraaminophthalocyanine-functionalized PbS nanostructures probed by transient absorption spectroscopy. *Angew. Chem. Int. Ed.* **2017**, *56*, 14061–14065. [CrossRef] [PubMed]
74. Nozik, A.J. Spectroscopy and hot electron relaxation dynamics in semiconductor quantum wells and quantum dots. *Annu. Rev. Phys. Chem.* **2001**, *52*, 193–231. [CrossRef] [PubMed]
75. Kambhampati, P. Hot exciton relaxation dynamics in semiconductor quantum dots: Radiationless transitions on the nanoscale. *J. Phys. Chem. C* **2011**, *115*, 22089–22109. [CrossRef]
76. Nozik, A.J. Exciton multiplication and relaxation dynamics in quantum dots: Applications to ultrahigh-efficiency solar photon conversion. *Inorg. Chem.* **2005**, *44*, 6893–6899. [CrossRef] [PubMed]
77. Beard, M.C.; Luther, J.M.; Semonin, O.E.; Nozik, A.J. Third generation photovoltaics based on multiple exciton generation in quantum confined semiconductors. *Acc. Chem. Res.* **2013**, *46*, 1252–1260. [CrossRef] [PubMed]
78. Gao, J.; Fidler, A.F.; Klimov, V.I. Carrier multiplication detected through transient photocurrent in device-grade films of lead selenide quantum dots. *Nat. Commun.* **2015**, *6*, 8185. [CrossRef] [PubMed]
79. Semonin, O.E.; Luther, J.M.; Choi, S.; Chen, H.-Y.; Gao, J.; Nozik, A.J.; Beard, M.C. Peak external photocurrent quantum efficiency exceeding 100% via meg in a quantum dot solar cell. *Science* **2011**, *334*, 1530–1533. [CrossRef] [PubMed]
80. Davis, N.J.L.K.; Bohm, M.L.; Tabachnyk, M.; Wisnivesky-Rocca-Rivarola, F.; Jellicoe, T.C.; Ducati, C.; Ehrler, B.; Greenham, N.C. Multiple-exciton generation in lead selenide nanorod solar cells with external quantum efficiencies exceeding 120%. *Nat. Commun.* **2015**, *6*, 8259. [CrossRef] [PubMed]
81. Böhm, M.L.; Jellicoe, T.C.; Tabachnyk, M.; Davis, N.J.L.K.; Wisnivesky-Rocca-Rivarola, F.; Ducati, C.; Ehrler, B.; Bakulin, A.A.; Greenham, N.C. Lead telluride quantum dot solar cells displaying external quantum efficiencies exceeding 120%. *Nano Lett.* **2015**, *15*, 7987–7993. [CrossRef] [PubMed]
82. Beard, M.C.; Ellingson, R.J. Multiple exciton generation in semiconductor nanocrystals: Toward efficient solar energy conversion. *Laser Photonics Rev.* **2008**, *2*, 377–399. [CrossRef]
83. Aerts, M.; Suchand Sandeep, C.S.; Gao, Y.; Savenije, T.J.; Schins, J.M.; Houtepen, A.J.; Kinge, S.; Siebbeles, L.D.A. Free charges produced by carrier multiplication in strongly coupled PbSe quantum dot films. *Nano Lett.* **2011**, *11*, 4485–4489. [CrossRef] [PubMed]
84. Yan, Y.; Crisp, R.W.; Gu, J.; Chernomordik, B.D.; Pach, G.F.; Marshall, A.R.; Turner, J.A.; Beard, M.C. Multiple exciton generation for photoelectrochemical hydrogen evolution reactions with quantum yields exceeding 100%. *Nat. Energy* **2017**, *2*, 17052. [CrossRef]
85. Spoor, F.C.M.; Grimaldi, G.; Delerue, C.; Evers, W.H.; Crisp, R.W.; Geiregat, P.; Hens, Z.; Houtepen, A.J.; Siebbeles, L.D.A. Asymmetric optical transitions determine the onset of carrier multiplication in lead chalcogenide quantum confined and bulk crystals. *ACS Nano* **2018**, *12*, 4796–4802. [CrossRef] [PubMed]
86. Cirloganu, C.M.; Padilha, L.A.; Lin, Q.; Makarov, N.S.; Velizhanin, K.A.; Luo, H.; Robel, I.; Pietryga, J.M.; Klimov, V.I. Enhanced carrier multiplication in engineered quasi-type-ii quantum dots. *Nat. Commun.* **2014**, *5*, 4148. [CrossRef] [PubMed]
87. Nanayakkara, S.U.; Cohen, G.; Jiang, C.-S.; Romero, M.J.; Maturova, K.; Al-Jassim, M.; van de Lagemaat, J.; Rosenwaks, Y.; Luther, J.M. Built-in potential and charge distribution within single heterostructured nanorods measured by scanning kelvin probe microscopy. *Nano Lett.* **2013**, *13*, 1278–1284. [CrossRef] [PubMed]

88. Nanayakkara, S.U.; van de Lagemaat, J.; Luther, J.M. Scanning probe characterization of heterostructured colloidal nanomaterials. *Chem. Rev.* **2015**, *115*, 8157–8181. [CrossRef] [PubMed]
89. Zhang, J.; Chernomordik, B.D.; Crisp, R.W.; Kroupa, D.M.; Luther, J.M.; Miller, E.M.; Gao, J.; Beard, M.C. Preparation of cd/pb chalcogenide heterostructured janus particles via controllable cation exchange. *ACS Nano* **2015**, *9*, 7151–7163. [CrossRef] [PubMed]
90. Kroupa, D.M.; Pach, G.F.; Vörös, M.; Giberti, F.; Chernomordik, B.D.; Crisp, R.W.; Nozik, A.J.; Johnson, J.C.; Singh, R.; Klimov, V.I.; et al. Enhanced multiple exciton generation in PbS | CdS janus-like heterostructured nanocrystals. *ACS Nano* **2018**. [CrossRef] [PubMed]
91. Grimaldi, G.; Crisp, R.W.; ten Brinck, S.; Zapata, F.; van Ouwendorp, M.; Renaud, N.; Kirkwood, N.; Evers, W.H.; Kinge, S.; Infante, I.; et al. Hot-electron transfer in quantum-dot heterojunction films. *Nat. Commun.* **2018**, *9*, 2310. [CrossRef] [PubMed]
92. Crisp, R.W.; Schrauben, J.N.; Beard, M.C.; Luther, J.M.; Johnson, J.C. Coherent exciton delocalization in strongly coupled quantum dot arrays. *Nano Lett.* **2013**, *13*, 4862–4869. [CrossRef] [PubMed]
93. Scholes, G.D.; Kim, J.; Wong, C.Y. Exciton spin relaxation in quantum dots measured using ultrafast transient polarization grating spectroscopy. *Phys. Rev. B* **2006**, *73*, 195325. [CrossRef]
94. Baumgardner, W.J.; Whitham, K.; Hanrath, T. Confined-but-connected quantum solids via controlled ligand displacement. *Nano Lett.* **2013**, *13*, 3225–3231. [CrossRef] [PubMed]
95. Crisp, R.W.; Pach, G.F.; Kurley, J.M.; France, R.M.; Reese, M.O.; Nanayakkara, S.U.; MacLeod, B.A.; Talapin, D.V.; Beard, M.C.; Luther, J.M. Tandem solar cells from solution-processed CdTe and PbS quantum dots using a ZnTe–ZnO tunnel junction. *Nano Lett.* **2017**, *17*, 1020–1027. [CrossRef] [PubMed]
96. Wang, X.; Koleilat, G.I.; Tang, J.; Liu, H.; Kramer, I.J.; Debnath, R.; Brzozowski, L.; Barkhouse, D.A.R.; Levina, L.; Hoogland, S.; et al. Tandem colloidal quantum dot solar cells employing a graded recombination layer. *Nat. Photonics* **2011**, *5*, 480–484. [CrossRef]
97. Choi, J.J.; Wenger, W.N.; Hoffman, R.S.; Lim, Y.-F.; Luria, J.; Jasieniak, J.; Marohn, J.A.; Hanrath, T. Solution-processed nanocrystal quantum dot tandem solar cells. *Adv. Mater.* **2011**, *23*, 3144–3148. [CrossRef] [PubMed]
98. Bi, Y.; Pradhan, S.; Akgul, M.Z.; Gupta, S.; Stavrinadis, A.; Wang, J.; Konstantatos, G. Colloidal quantum dot tandem solar cells using chemical vapor deposited graphene as an atomically thin intermediate recombination layer. *ACS Energy Lett.* **2018**, *3*, 1753–1759. [CrossRef]
99. König, D.; Casalenuovo, K.; Takeda, Y.; Conibeer, G.; Guillemoles, J.F.; Patterson, R.; Huang, L.M.; Green, M.A. Hot carrier solar cells: Principles, materials and design. *Phys. E Low-Dimens. Syst. Nanostruct.* **2010**, *42*, 2862–2866. [CrossRef]
100. Pandey, A.; Guyot-Sionnest, P. Slow electron cooling in colloidal quantum dots. *Science* **2008**, *322*, 929–932. [CrossRef] [PubMed]
101. Efros, A.L.; Kharchenko, V.A.; Rosen, M. Breaking the phonon bottleneck in nanometer quantum dots: Role of auger-like processes. *Solid State Commun.* **1995**, *93*, 281–284. [CrossRef]
102. Guyot-Sionnest, P.; Wehrenberg, B.; Yu, D. Intraband relaxation in CdSe nanocrystals and the strong influence of the surface ligands. *J. Chem. Phys.* **2005**, *123*, 074709. [CrossRef] [PubMed]
103. Sewall, S.L.; Cooney, R.R.; Anderson, K.E.H.; Dias, E.A.; Kambhampati, P. State-to-state exciton dynamics in semiconductor quantum dots. *Phys. Rev. B* **2006**, *74*, 235328. [CrossRef]
104. Bozyigit, D.; Yazdani, N.; Yarema, M.; Yarema, O.; Lin, W.M.M.; Volk, S.; Vuttivorakulchai, K.; Luisier, M.; Juranyi, F.; Wood, V. Soft surfaces of nanomaterials enable strong phonon interactions. *Nature* **2016**, *531*, 618–622. [CrossRef] [PubMed]
105. Yazdani, N.; Bozyigit, D.; Vuttivorakulchai, K.; Luisier, M.; Infante, I.; Wood, V. Tuning electron–phonon interactions in nanocrystals through surface termination. *Nano Lett.* **2018**, *18*, 2233–2242. [CrossRef] [PubMed]
106. Kershaw, S.; Rogach, A. Carrier multiplication mechanisms and competing processes in colloidal semiconductor nanostructures. *Materials* **2017**, *10*, 1095. [CrossRef] [PubMed]
107. Smith, C.; Binks, D. Multiple exciton generation in colloidal nanocrystals. *Nanomaterials* **2014**, *4*, 19–45. [CrossRef] [PubMed]
108. Spoor, F.C.M.; Kunneman, L.T.; Evers, W.H.; Renaud, N.; Grozema, F.C.; Houtepen, A.J.; Siebbeles, L.D.A. Hole cooling is much faster than electron cooling in PbSe quantum dots. *ACS Nano* **2016**, *10*, 695–703. [CrossRef] [PubMed]

109. Scheele, M. To be or not to be: Band-like transport in quantum dot solids. *Z. Phys. Chem.* **2015**, *229*, 167–178. [CrossRef]
110. Gao, Y.; Talgorn, E.; Aerts, M.; Trinh, M.T.; Schins, J.M.; Houtepen, A.J.; Siebbeles, L.D.A. Enhanced hot-carrier cooling and ultrafast spectral diffusion in strongly coupled PbSe quantum-dot solids. *Nano Lett.* **2011**, *11*, 5471–5476. [CrossRef] [PubMed]
111. Chernomordik, B.D.; Marshall, A.R.; Pach, G.F.; Luther, J.M.; Beard, M.C. Quantum dot solar cell fabrication protocols. *Chem. Mater.* **2016**, *29*, 189–198. [CrossRef]
112. Kim, J.Y.; Adinolfi, V.; Sutherland, B.R.; Voznyy, O.; Kwon, S.J.; Kim, T.W.; Kim, J.; Ihee, H.; Kemp, K.; Adachi, M.; et al. Single-step fabrication of quantum funnels via centrifugal colloidal casting of nanoparticle films. *Nat. Commun.* **2015**, *6*, 7772. [CrossRef] [PubMed]
113. Kramer, I.J.; Levina, L.; Debnath, R.; Zhitomirsky, D.; Sargent, E.H. Solar cells using quantum funnels. *Nano Lett.* **2011**, *11*, 3701–3706. [CrossRef] [PubMed]
114. Gao, Y.; Sandeep, C.S.S.; Schins, J.M.; Houtepen, A.J.; Siebbeles, L.D.A. Disorder strongly enhances auger recombination in conductive quantum-dot solids. *Nat. Commun.* **2013**, *4*, 2329. [CrossRef] [PubMed]
115. Gomez-Campos, F.M.; Rodriguez-Bolivar, S.; Skibinsky-Gitlin, E.S.; Califano, M. Efficient, non-stochastic, monte-carlo-like-accurate method for the calculation of the temperature-dependent mobility in nanocrystal films. *Nanoscale* **2018**, *10*, 9679–9690. [CrossRef] [PubMed]
116. Gilmore, R.H.; Winslow, S.W.; Lee, E.M.Y.; Ashner, M.N.; Yager, K.G.; Willard, A.P.; Tisdale, W.A. Inverse temperature dependence of charge carrier hopping in quantum dot solids. *ACS Nano* **2018**, *12*, 7741–7749. [CrossRef] [PubMed]
117. Gilmore, R.H.; Lee, E.M.Y.; Weidman, M.C.; Willard, A.P.; Tisdale, W.A. Charge carrier hopping dynamics in homogeneously broadened PbS quantum dot solids. *Nano Lett.* **2017**, *17*, 893–901. [CrossRef] [PubMed]
118. Gao, Y.; Aerts, M.; Sandeep, C.S.S.; Talgorn, E.; Savenije, T.J.; Kinge, S.; Siebbeles, L.D.A.; Houtepen, A.J. Photoconductivity of PbSe quantum-dot solids: Dependence on ligand anchor group and length. *ACS Nano* **2012**, *6*, 9606–9614. [CrossRef] [PubMed]
119. Talgorn, E.; Gao, Y.; Aerts, M.; Kunneman, L.T.; Schins, J.M.; Savenije, T.J.; van HuisMarijn, A.; van der ZantHerre, S.J.; Houtepen, A.J.; Siebbeles, L.D.A. Unity quantum yield of photogenerated charges and band-like transport in quantum-dot solids. *Nat. Nanotechnol.* **2011**, *6*, 733–739. [CrossRef] [PubMed]
120. Lee, J.-S.; Kovalenko, M.V.; Huang, J.; Chung, D.S.; Talapin, D.V. Band-like transport, high electron mobility and high photoconductivity in all-inorganic nanocrystal arrays. *Nat. Nanotechnol.* **2011**, *6*, 348–352. [CrossRef] [PubMed]
121. Sakanoue, T.; Sirringhaus, H. Band-like temperature dependence of mobility in a solution-processed organic semiconductor. *Nat. Mater.* **2010**, *9*, 736–740. [CrossRef] [PubMed]
122. Sandeep, C.S.S.; Cate, S.t.; Schins, J.M.; Savenije, T.J.; Liu, Y.; Law, M.; Kinge, S.; Houtepen, A.J.; Siebbeles, L.D.A. High charge-carrier mobility enables exploitation of carrier multiplication in quantum-dot films. *Nat. Commun.* **2013**, *4*, 2360. [CrossRef] [PubMed]
123. Anderson, N.C.; Hendricks, M.P.; Choi, J.J.; Owen, J.S. Ligand exchange and the stoichiometry of metal chalcogenide nanocrystals: Spectroscopic observation of facile metal-carboxylate displacement and binding. *J. Am. Chem. Soc.* **2013**, *135*, 18536–18548. [CrossRef] [PubMed]
124. ten Cate, S.; Liu, Y.; Suchand Sandeep, C.; Kinge, S.; Houtepen, A.J.; Savenije, T.J.; Schins, J.M.; Law, M.; Siebbeles, L.D. Activating carrier multiplication in PbSe quantum dot solids by infilling with atomic layer deposition. *J. Phys. Chem. Lett.* **2013**, *4*, 1766–1770. [CrossRef] [PubMed]
125. Zhitomirsky, D.; Voznyy, O.; Levina, L.; Hoogland, S.; Kemp, K.W.; Ip, A.H.; Thon, S.M.; Sargent, E.H. Engineering colloidal quantum dot solids within and beyond the mobility-invariant regime. *Nat. Commun.* **2014**, *5*, 3803. [CrossRef] [PubMed]
126. Crisp, R.W.; Callahan, R.; Reid, O.G.; Dolzhnikov, D.S.; Talapin, D.V.; Rumbles, G.; Luther, J.M.; Kopidakis, N. Photoconductivity of CdTe nanocrystal-based thin films: Te(2–) ligands lead to charge carrier diffusion lengths over 2 μm. *J. Phys. Chem. Lett.* **2015**, *6*, 4815–4821. [CrossRef] [PubMed]
127. Liu, Y.; Gibbs, M.; Puthussery, J.; Gaik, S.; Ihly, R.; Hillhouse, H.W.; Law, M. Dependence of carrier mobility on nanocrystal size and ligand length in PbSe nanocrystal solids. *Nano Lett.* **2010**, *10*, 1960–1969. [CrossRef] [PubMed]

128. Jeong, K.S.; Tang, J.; Liu, H.; Kim, J.; Schaefer, A.W.; Kemp, K.; Levina, L.; Wang, X.; Hoogland, S.; Debnath, R.; et al. Enhanced mobility-lifetime products in PbS colloidal quantum dot photovoltaics. *ACS Nano* **2012**, *6*, 89–99. [CrossRef] [PubMed]
129. Guyot-Sionnest, P.; Roberts, J.A. Background limited mid-infrared photodetection with photovoltaic hgte colloidal quantum dots. *Appl. Phys. Lett.* **2015**, *107*, 253104. [CrossRef]
130. Keuleyan, S.; Lhuillier, E.; Brajuskovic, V.; Guyot-Sionnest, P. Mid-infrared hgte colloidal quantum dot photodetectors. *Nat. Photonics* **2011**, *5*, 489. [CrossRef]
131. Miller, A.; Abrahams, E. Impurity conduction at low concentrations. *Physical Review* **1960**, *120*, 745–755. [CrossRef]
132. Delerue, C.; Lannoo, M. *Nanostructures: Theory and Modeling*; Springer: New York, NY, USA, 2004.
133. Bruggeman, D. Calculation of various physics constants in heterogenous substances i dielectricity constants and conductivity of mixed bodies from isotropic substances. *Ann. Phys.* **1935**, *24*, 636–664. [CrossRef]
134. Swart, I.; Sun, Z.; Vanmaekelbergh, D.; Liljeroth, P. Hole-induced electron transport through core−shell quantum dots: A direct measurement of the electron−hole interaction. *Nano Lett.* **2010**, *10*, 1931–1935. [CrossRef] [PubMed]
135. Marino, E.; Kodger, T.E.; Crisp, R.W.; Timmerman, D.; MacArthur, K.E.; Heggen, M.; Schall, P. Repairing nanoparticle surface defects. *Angew. Chem.* **2017**, *129*, 13983–13987. [CrossRef]
136. Gao, J.; Zhang, J.; van de Lagemaat, J.; Johnson, J.C.; Beard, M.C. Charge generation in PbS quantum dot solar cells characterized by temperature-dependent steady-state photoluminescence. *ACS Nano* **2014**, *8*, 12814–12825. [CrossRef] [PubMed]
137. Carey, G.H.; Levina, L.; Comin, R.; Voznyy, O.; Sargent, E.H. Record charge carrier diffusion length in colloidal quantum dot solids via mutual dot-to-dot surface passivation. *Adv. Mater.* **2015**, *27*, 3325–3330. [CrossRef] [PubMed]
138. Yang, Y.; Yang, M.; Li, Z.; Crisp, R.; Zhu, K.; Beard, M.C. Comparison of recombination dynamics in $CH_3NH_3PbBr_3$ and $CH_3NH_3PbI_3$ perovskite films: Influence of exciton binding energy. *J. Phys. Chem. Lett.* **2015**, *6*, 4688–4692. [CrossRef] [PubMed]
139. Pietryga, J.M.; Park, Y.-S.; Lim, J.; Fidler, A.F.; Bae, W.K.; Brovelli, S.; Klimov, V.I. Spectroscopic and device aspects of nanocrystal quantum dots. *Chem. Rev.* **2016**, *116*, 10513–10622. [CrossRef] [PubMed]
140. Marshall, A.R.; Beard, M.C.; Johnson, J.C. Nongeminate radiative recombination of free charges in cation-exchanged PbS quantum dot films. *Chem. Phys.* **2015**, *471*, 75–80. [CrossRef]
141. Geiregat, P.; Houtepen, A.J.; Sagar, L.K.; Infante, I.; Zapata, F.; Grigel, V.; Allan, G.; Delerue, C.; Van Thourhout, D.; Hens, Z. Continuous-wave infrared optical gain and amplified spontaneous emission at ultralow threshold by colloidal hgte quantum dots. *Nat. Mater.* **2017**, *17*, 35. [CrossRef] [PubMed]
142. Klimov, V.I. Mechanisms for photogeneration and recombination of multiexcitons in semiconductor nanocrystals: Implications for lasing and solar energy conversion. *J. Phys. Chem. B* **2006**, *110*, 16827–16845. [CrossRef] [PubMed]
143. Wu, K.; Park, Y.-S.; Lim, J.; Klimov, V.I. Towards zero-threshold optical gain using charged semiconductor quantum dots. *Nat. Nanotechnol.* **2017**, *12*, 1140. [CrossRef] [PubMed]
144. Crisp, R.W.; Kroupa, D.M.; Marshall, A.R.; Miller, E.M.; Zhang, J.; Beard, M.C.; Luther, J.M. Metal halide solid-state surface treatment for high efficiency PbS and PbSe qd solar cells. *Sci. Rep.* **2015**, *5*, 9945. [CrossRef] [PubMed]
145. Brown, P.R.; Kim, D.; Lunt, R.R.; Zhao, N.; Bawendi, M.G.; Grossman, J.C.; Bulović, V. Energy level modification in lead sulfide quantum dot thin films through ligand exchange. *ACS Nano* **2014**, *8*, 5863–5872. [CrossRef] [PubMed]
146. Deng, Z.; Jeong, K.S.; Guyot-Sionnest, P. Colloidal quantum dots intraband photodetectors. *ACS Nano* **2014**, *8*, 11707–11714. [CrossRef] [PubMed]
147. Tang, X.; Tang, X.; Lai, K.W.C. Scalable fabrication of infrared detectors with multispectral photoresponse based on patterned colloidal quantum dot films. *ACS Photonics* **2016**, *3*, 2396–2404. [CrossRef]
148. Cho, Y.; Hou, B.; Lim, J.; Lee, S.; Pak, S.; Hong, J.; Giraud, P.; Jang, A.R.; Lee, Y.-W.; Lee, J.; et al. Balancing charge carrier transport in a quantum dot p–n junction toward hysteresis-free high-performance solar cells. *ACS Energy Lett.* **2018**, *3*, 1036–1043. [CrossRef] [PubMed]

149. Crisp, R.W.; Panthani, M.G.; Rance, W.L.; Duenow, J.N.; Parilla, P.A.; Callahan, R.; Dabney, M.S.; Berry, J.J.; Talapin, D.V.; Luther, J.M. Nanocrystal grain growth and device architectures for high-efficiency CdTe ink-based photovoltaics. *ACS Nano* **2014**, *8*, 9063–9072. [CrossRef] [PubMed]
150. Kurley, J.M.; Panthani, M.G.; Crisp, R.W.; Nanayakkara, S.U.; Pach, G.F.; Reese, M.O.; Hudson, M.H.; Dolzhnikov, D.S.; Tanygin, V.; Luther, J.M.; et al. Transparent ohmic contacts for solution-processed, ultrathin CdTe solar cells. *ACS Energy Lett.* **2017**, *2*, 270–278. [CrossRef]
151. Kagan, C.R.; Lifshitz, E.; Sargent, E.H.; Talapin, D.V. Building devices from colloidal quantum dots. *Science* **2016**, *353*, aac5523. [CrossRef] [PubMed]
152. O'Regan, B.; Grätzel, M. A low-cost, high-efficiency solar cell based on dye-sensitized colloidal tio2 films. *Nature* **1991**, *353*, 737. [CrossRef]
153. Hoyer, P.; Könenkamp, R. Photoconduction in porous tio2 sensitized by PbS quantum dots. *Appl. Phys. Lett.* **1995**, *66*, 349–351. [CrossRef]
154. Ju, T.; Graham, R.L.; Zhai, G.; Rodriguez, Y.W.; Breeze, A.J.; Yang, L.; Alers, G.B.; Carter, S.A. High efficiency mesoporous titanium oxide PbS quantum dot solar cells at low temperature. *Appl. Phys. Lett.* **2010**, *97*, 043106. [CrossRef]
155. Olle, I. Organic photovoltaics over three decades. *Adv. Mater.* **2018**, *30*, 1800388.
156. Im, S.H.; Kim, H.J.; Kim, S.W.; Kim, S.W.; Seok, S.I. All solid state multiply layered PbS colloidal quantum-dot-sensitized photovoltaic cells. *Energy Environ. Sci.* **2011**, *4*, 4181–4186. [CrossRef]
157. Zhang, Z.; Shi, C.; Lv, K.; Ma, C.; Xiao, G.; Ni, L. 200-nm long tio2 nanorod arrays for efficient solid-state PbS quantum dot-sensitized solar cells. *J. Energy Chem.* **2017**, *27*, 1214–1218. [CrossRef]
158. Zhang, Z.; Shi, C.; Xiao, G.; Lv, K.; Ma, C.; Yue, J. All-solid-state quantum-dot-sensitized solar cells with compact PbS quantum-dot thin films and tio2 nanorod arrays. *Ceram. Int.* **2017**, *43*, 10052–10056. [CrossRef]
159. Zhang, Z.; Shi, C.; Chen, J.; Xiao, G.; Li, L. Combination of short-length tio2 nanorod arrays and compact PbS quantum-dot thin films for efficient solid-state quantum-dot-sensitized solar cells. *Appl. Surf. Sci.* **2017**, *410*, 8–13. [CrossRef]
160. Lee, J.W.; Son, D.Y.; Ahn, T.K.; Shin, H.W.; Kim, I.Y.; Hwang, S.J.; Ko, M.J.; Sul, S.; Han, H.; Park, N.G. Quantum-dot-sensitized solar cell with unprecedentedly high photocurrent. *Sci. Rep.* **2013**, *3*, 1–8. [CrossRef] [PubMed]
161. Jiao, S.; Wang, J.; Shen, Q.; Li, Y.; Zhong, X. Surface engineering of PbS quantum dot sensitized solar cells with a conversion efficiency exceeding 7%. *J. Mater. Chem. A* **2016**, *4*, 7214–7221. [CrossRef]
162. Yu, J.; Wang, W.; Pan, Z.; Du, J.; Ren, Z.; Xue, W.; Zhong, X. Quantum dot sensitized solar cells with efficiency over 12% based on tetraethyl orthosilicate additive in polysulfide electrolyte. *J. Mater. Chem. A* **2017**, *5*, 14124–14133. [CrossRef]
163. Rühle, S.; Shalom, M.; Zaban, A. Quantum-dot-sensitized solar cells. *ChemPhysChem* **2010**, *11*, 2290–2304. [CrossRef] [PubMed]
164. Duan, J.; Zhang, H.; Tang, Q.; He, B.; Yu, L. Recent advances in critical materials for quantum dot-sensitized solar cells: A review. *J. Mater. Chem. A* **2015**, *3*, 17497–17510. [CrossRef]
165. Zhao, K.; Pan, Z.; Mora-Seró, I.; Cánovas, E.; Wang, H.; Song, Y.; Gong, X.; Wang, J.; Bonn, M.; Bisquert, J.; et al. Boosting power conversion efficiencies of quantum-dot-sensitized solar cells beyond 8% by recombination control. *J. Am. Chem. Soc.* **2015**, *137*, 5602–5609. [CrossRef] [PubMed]
166. Johnston, K.W.; Pattantyus-Abraham, A.G.; Clifford, J.P.; Myrskog, S.H.; Hoogland, S.; Shukla, H.; Klem, E.J.D.; Levina, L.; Sargent, E.H. Efficient schottky-quantum-dot photovoltaics: The roles of depletion, drift, and diffusion. *Appl. Phys. Lett.* **2008**, *92*, 122111. [CrossRef]
167. Luther, J.M.; Law, M.; Beard, M.C.; Song, Q.; Reese, M.O.; Ellingson, R.J.; Nozik, A.J. Schottky solar cells based on colloidal nanocrystal films. *Nano Lett.* **2008**, *8*, 3488–3492. [CrossRef] [PubMed]
168. Koleilat, G.I.; Levina, L.; Shukla, H.; Myrskog, S.H.; Hinds, S.; Pattantyus-Abraham, A.G.; Sargent, E.H. Efficient, stable infrared photovoltaics based on solution-cast colloidal quantum dots. *ACS Nano* **2008**, *2*, 833–840. [CrossRef] [PubMed]
169. Johnston, K.W.; Pattantyus-Abraham, A.G.; Clifford, J.P.; Myrskog, S.H.; MacNeil, D.D.; Levina, L.; Sargent, E.H. Schottky-quantum dot photovoltaics for efficient infrared power conversion. *Appl. Phys. Lett.* **2008**, *92*, 151115. [CrossRef]
170. Yoon, W.; Boercker, J.E.; Lumb, M.P.; Placencia, D.; Foos, E.E.; Tischler, J.G. Enhanced open-circuit voltage of PbS nanocrystal quantum dot solar cells. *Sci. Rep.* **2013**, *3*, 2225. [CrossRef] [PubMed]

171. Dubey, P.K.; Paranjape, V.V. Open-circuit voltage of a schottky-barrier solar cell. *J. Appl. Phys.* **1977**, *48*, 324–328. [CrossRef]
172. Pattantyus-Abraham, A.G.; Kramer, I.J.; Barkhouse, A.R.; Wang, X.; Konstantatos, G.; Debnath, R.; Levina, L.; Raabe, I.; Nazeeruddin, M.K.; Grätzel, M.; et al. Depleted-heterojunction colloidal quantum dot solar cells. *ACS Nano* **2010**, *4*, 3374–3380. [CrossRef] [PubMed]
173. Miller, E.M.; Kroupa, D.M.; Zhang, J.; Schulz, P.; Marshall, A.R.; Kahn, A.; Lany, S.; Luther, J.M.; Beard, M.C.; Perkins, C.L.; et al. Revisiting the valence and conduction band size dependence of PbS quantum dot thin films. *ACS Nano* **2016**, *10*, 3302–3311. [CrossRef] [PubMed]
174. Chuang, C.-H.M.; Brown, P.R.; Bulović, V.; Bawendi, M.G. Improved performance and stability in quantum dot solar cells through band alignment engineering. *Nat. Mater.* **2014**, *13*, 796–801. [CrossRef] [PubMed]
175. Kirmani, A.R.; Kiani, A.; Said, M.M.; Voznyy, O.; Wehbe, N.; Walters, G.; Barlow, S.; Sargent, E.H.; Marder, S.R.; Amassian, A. Remote molecular doping of colloidal quantum dot photovoltaics. *ACS Energy Lett.* **2016**, *1*, 922–930. [CrossRef]
176. Kirmani, A.R.; García De Arquer, F.P.; Fan, J.Z.; Khan, J.I.; Walters, G.; Hoogland, S.; Wehbe, N.; Said, M.M.; Barlow, S.; Laquai, F.; et al. Molecular doping of the hole-transporting layer for efficient, single-step-deposited colloidal quantum dot photovoltaics. *ACS Energy Lett.* **2017**, *2*, 1952–1959. [CrossRef]
177. Kroupa, D.M.; Vörös, M.; Brawand, N.P.; McNichols, B.W.; Miller, E.M.; Gu, J.; Nozik, A.J.; Sellinger, A.; Galli, G.; Beard, M.C. Tuning colloidal quantum dot band edge positions through solution-phase surface chemistry modification. *Nat. Commun.* **2017**, *8*, 15257. [CrossRef] [PubMed]
178. Martín-García, B.; Bi, Y.; Prato, M.; Spirito, D.; Krahne, R.; Konstantatos, G.; Moreels, I. Reduction of moisture sensitivity of PbS quantum dot solar cells by incorporation of reduced graphene oxide. *Sol. Energy Mater. Sol. Cells* **2018**, *183*, 1–7. [CrossRef]
179. McDonald, S.A.; Konstantatos, G.; Zhang, S.; Cyr, P.W.; Klem, E.J.D.; Levina, L.; Sargent, E.H. Solution-processed PbS quantum dot infrared photodetectors and photovoltaics. *Nat. Mater.* **2005**, *4*, 138. [CrossRef] [PubMed]
180. Fritz, K.P.; Guenes, S.; Luther, J.; Kumar, S.; Sariciftci, N.S.; Scholes, G.D. Iv–vi nanocrystal–polymer solar cells. *J. Photochem. Photobiol. A Chem.* **2008**, *195*, 39–46. [CrossRef]
181. Lan, X.; Voznyy, O.; Kiani, A.; García De Arquer, F.P.; Abbas, A.S.; Kim, G.H.; Liu, M.; Yang, Z.; Walters, G.; Xu, J.; et al. Passivation using molecular halides increases quantum dot solar cell performance. *Adv. Mater.* **2016**, *28*, 299–304. [CrossRef] [PubMed]
182. Lan, X.; Voznyy, O.; García De Arquer, F.P.; Liu, M.; Xu, J.; Proppe, A.H.; Walters, G.; Fan, F.; Tan, H.; Liu, M.; et al. 10.6% certified colloidal quantum dot solar cells via solvent-polarity-engineered halide passivation. *Nano Lett.* **2016**, *16*, 4630–4634. [CrossRef] [PubMed]
183. Azmi, R.; Sinaga, S.; Aqoma, H.; Seo, G.; Kyu, T.; Park, M. Highly efficient air-stable colloidal quantum dot solar cells by improved surface trap passivation. *Nano Energy* **2017**, *39*, 86–94. [CrossRef]
184. Azmi, R.; Nam, S.Y.; Sinaga, S.; Oh, S.H.; Ahn, T.K.; Yoon, S.C.; Jung, I.H.; Jang, S.Y. Improved performance of colloidal quantum dot solar cells using high-electric-dipole self-assembled layers. *Nano Energy* **2017**, *39*, 355–362. [CrossRef]
185. Hu, L.; Zhang, Z.; Patterson, R.J.; Hu, Y.; Chen, W.; Chen, C.; Li, D.; Hu, C.; Ge, C.; Chen, Z.; et al. Achieving high-performance PbS quantum dot solar cells by improving hole extraction through ag doping. *Nano Energy* **2018**, *46*, 212–219. [CrossRef]
186. Ding, C.; Zhang, Y.; Liu, F.; Kitabatake, Y.; Hayase, S. Understanding charge transfer and recombination by interface engineering for improving the efficiency of PbS quantum dot solar cells. *Nanoscale Horiz.* **2018**, *3*, 417–429. [CrossRef]
187. Konstantatos, G. Suppressing deep traps in PbS colloidal. *ACS Energy Lett.* **2017**, *2*, 739–744.
188. Pradhan, S.; Stavrinadis, A.; Gupta, S.; Konstantatos, G. Reducing interface recombination through mixed nanocrystal interlayers in PbS quantum dot solar cells. *ACS Appl. Mater. Interfaces* **2017**, *9*, 27390–27395. [CrossRef] [PubMed]
189. Yang, Z.; Fan, J.Z.; Proppe, A.H.; De Arquer, F.P.G.; Rossouw, D.; Voznyy, O.; Lan, X.; Liu, M.; Walters, G.; Quintero-Bermudez, R.; et al. Mixed-quantum-dot solar cells. *Nat. Commun.* **2017**, *8*, 1–9. [CrossRef] [PubMed]

190. Zhang, X.; Zhang, J.; Phuyal, D.; Du, J.; Tian, L.; Öberg, V.A.; Johansson, M.B.; Cappel, U.B.; Karis, O.; Liu, J.; et al. Inorganic $CsPbI_3$ perovskite coating on PbS quantum dot for highly efficient and stable infrared light converting solar cells. *Adv. Energy Mater.* **2018**, *8*, 1–11. [CrossRef]
191. Liu, M.; De Arquer, F.P.G.; Li, Y.; Lan, X.; Kim, G.H.; Voznyy, O.; Jagadamma, L.K.; Abbas, A.S.; Hoogland, S.; Lu, Z.; et al. Double-sided junctions enable high-performance colloidal-quantum-dot photovoltaics. *Adv. Mater.* **2016**, *28*, 4142–4148. [CrossRef] [PubMed]
192. Choi, J.; Kim, Y.; Jo, J.W.; Kim, J.; Sun, B.; Walters, G.; García de Arquer, F.P.; Quintero-Bermudez, R.; Li, Y.; Tan, C.S.; et al. Chloride passivation of ZnO electrodes improves charge extraction in colloidal quantum dot photovoltaics. *Adv. Mater.* **2017**, *29*, 1702350. [CrossRef] [PubMed]
193. Liu, M.; Voznyy, O.; Sabatini, R.; García De Arquer, F.P.; Munir, R.; Balawi, A.H.; Lan, X.; Fan, F.; Walters, G.; Kirmani, A.R.; et al. Hybrid organic-inorganic inks flatten the energy landscape in colloidal quantum dot solids. *Nat. Mater.* **2017**, *16*, 258–263. [CrossRef] [PubMed]
194. Wang, Y.; Lu, K.; Han, L.; Liu, Z.; Shi, G.; Fang, H.; Chen, S.; Wu, T.; Yang, F.; Gu, M.; et al. In situ passivation for efficient PbS quantum dot solar cells by precursor engineering. *Adv. Mater.* **2018**, *1704871*, 1–8. [CrossRef] [PubMed]
195. Lu, K.; Wang, Y.; Liu, Z.; Han, L.; Shi, G.; Fang, H.; Chen, J.; Ye, X.; Chen, S.; Yang, F.; et al. High-efficiency PbS quantum-dot solar cells with greatly simplified fabrication processing via "solvent-curing". *Adv. Mater.* **2018**, *1707572*, 1–9. [CrossRef] [PubMed]
196. Jin, Z.; Yuan, M.; Li, H.; Yang, H.; Zhou, Q.; Liu, H.; Lan, X.; Liu, M.; Wang, J.; Sargent, E.H.; et al. Graphdiyne: An efficient hole transporter for stable high-performance colloidal quantum dot solar cells. *Adv. Funct. Mater.* **2016**, *26*, 5284–5289. [CrossRef]
197. Kim, G.H.; García De Arquer, F.P.; Yoon, Y.J.; Lan, X.; Liu, M.; Voznyy, O.; Yang, Z.; Fan, F.; Ip, A.H.; Kanjanaboos, P.; et al. High-efficiency colloidal quantum dot photovoltaics via robust self-assembled monolayers. *Nano Lett.* **2015**, *15*, 7691–7696. [CrossRef] [PubMed]
198. Goswami, P.N.; Mandal, D.; Rath, A.K. The role of surface ligands in determining the electronic properties of quantum dot solids and their impact on photovoltaic figure of merits. *Nanoscale* **2018**, *10*, 1072–1080. [CrossRef] [PubMed]
199. Pradhan, S.; Stavrinadis, A.; Gupta, S.; Bi, Y.; Di Stasio, F.; Konstantatos, G. Trap-state suppression and improved charge transport in PbS quantum dot solar cells with synergistic mixed-ligand treatments. *Small* **2017**, *13*, 1700598. [CrossRef] [PubMed]
200. Ip, A.H.; Kiani, A.; Kramer, I.J.; Voznyy, O.; Movahed, H.F.; Levina, L.; Adachi, M.M.; Hoogland, S.; Sargent, E.H. Infrared colloidal quantum dot photovoltaics via coupling enhancement and agglomeration suppression. *ACS Nano* **2015**, *9*, 8833–8842. [CrossRef] [PubMed]
201. Ip, A.H.; Thon, S.M.; Hoogland, S.; Voznyy, O.; Zhitomirsky, D.; Debnath, R.; Levina, L.; Rollny, L.R.; Carey, G.H.; Fischer, A.; et al. Hybrid passivated colloidal quantum dot solids. *Nat. Nanotechnol.* **2012**, *7*, 577–582. [CrossRef] [PubMed]
202. Ning, Z.; Ren, Y.; Hoogland, S.; Voznyy, O.; Levina, L.; Stadler, P.; Lan, X.; Zhitomirsky, D.; Sargent, E.H. All-inorganic colloidal quantum dot photovoltaics employing solution-phase halide passivation. *Adv. Mater.* **2012**, *24*, 6295–6299. [CrossRef] [PubMed]
203. Ning, Z.; Voznyy, O.; Pan, J.; Hoogland, S.; Adinolfi, V.; Xu, J.; Li, M.; Kirmani, A.R.; Sun, J.-P.; Minor, J.; et al. Air-stable n-type colloidal quantum dot solids. *Nat. Mater.* **2014**, *13*, 822–828. [CrossRef] [PubMed]
204. Ning, Z.; Dong, H.; Zhang, Q.; Voznyy, O.; Sargent, E.H. Solar cells based on inks of n-type colloidal quantum dots. *ACS Nano* **2014**, *8*, 10321–10327. [CrossRef] [PubMed]
205. Dirin, D.N.; Dreyfuss, S.; Bodnarchuk, M.I.; Nedelcu, G.; Papagiorgis, P.; Itskos, G.; Kovalenko, M.V. Lead halide perovskites and other metal halide complexes as inorganic capping ligands for colloidal nanocrystals. *J. Am. Chem. Soc.* **2014**, *136*, 6550–6553. [CrossRef] [PubMed]
206. Lai, L.-H.; Speirs, M.J.; Chang, F.-K.; Piveteau, L.; Kovalenko, M.V.; Chen, J.-S.; Wu, J.-J.; Loi, M.A. Increasing photon absorption and stability of PbS quantum dot solar cells using a ZnO interlayer. *Appl. Phys. Lett.* **2015**, *107*, 183901. [CrossRef]
207. Kiani, A.; Sutherland, B.R.; Kim, Y.; Ouellette, O.; Levina, L.; Walters, G.; Dinh, C.T.; Liu, M.; Voznyy, O.; Lan, X.; et al. Single-step colloidal quantum dot films for infrared solar harvesting. *Appl. Phys. Lett.* **2016**, *109*, 183105. [CrossRef]

208. Willis, S.M.; Cheng, C.; Assender, H.E.; Watt, A.A.R. The transitional heterojunction behavior of PbS/ZnO colloidal quantum dot solar cells. *Nano Lett.* **2012**, *12*, 1522–1526. [CrossRef] [PubMed]
209. Speirs, M.J.; Balazs, D.M.; Dirin, D.N.; Kovalenko, M.V.; Loi, M.A. Increased efficiency in pn-junction PbS QD solar cells via nahs treatment of the p-type layer. *Appl. Phys. Lett.* **2017**, *110*, 103904. [CrossRef]
210. Xu, J.; Wang, H.; Wang, Y.; Yang, S.; Ni, G.; Zou, B. Efficiency enhancement for solution-processed PbS quantum dots solar cells by inserting graphene oxide as hole-transporting and interface modifying layer. *Org. Electron. Phys. Mater. Appl.* **2018**, *58*, 270–275. [CrossRef]
211. Zhang, Y.; Wu, G.; Mora-Seró, I.; Ding, C.; Liu, F.; Huang, Q.; Ogomi, Y.; Hayase, S.; Toyoda, T.; Wang, R.; et al. Improvement of photovoltaic performance of colloidal quantum dot solar cells using organic small molecule as hole-selective layer. *J. Phys. Chem. Lett.* **2017**, *8*, 2163–2169. [CrossRef] [PubMed]
212. Ren, Z.; Kuang, Z.; Zhang, L.; Sun, J.; Yi, X.; Pan, Z.; Zhong, X.; Hu, J.; Xia, A.; Wang, J. Enhancing electron and hole extractions for efficient PbS quantum dot solar cells. *Sol. RRL* **2017**, *1*, 1700176. [CrossRef]
213. Jeong, Y.J.; Song, J.H.; Jeong, S.; Baik, S.J. PbS colloidal quantum dot solar cells with organic hole transport layers for enhanced carrier separation and ambient stability. *IEEE J. Photovolt.* **2018**, *8*, 493–498. [CrossRef]
214. Zhao, T.; Goodwin, E.D.; Guo, J.; Wang, H.; Diroll, B.T.; Murray, C.B.; Kagan, C.R. Advanced architecture for colloidal PbS quantum dot solar cells exploiting a CdSe quantum dot buffer layer. *ACS Nano* **2016**, *10*, 9267–9273. [CrossRef] [PubMed]
215. Zhang, X.; Johansson, E.M.J. Reduction of charge recombination in PbS colloidal quantum dot solar cells at the quantum dot/ZnO interface by inserting a mgZnO buffer layer. *J. Mater. Chem. A* **2017**, *5*, 303–310. [CrossRef]
216. Azmi, R.; Aqoma, H.; Hadmojo, W.T.; Yun, J.M.; Yoon, S.; Kim, K.; Do, Y.R.; Oh, S.H.; Jang, S.Y. Low-temperature-processed 9% colloidal quantum dot photovoltaic devices through interfacial management of p-n heterojunction. *Adv. Energy Mater.* **2016**, *6*, 1–10. [CrossRef]
217. Hu, L.; Patterson, R.J.; Hu, Y.; Chen, W.; Zhang, Z.; Yuan, L.; Chen, Z.; Conibeer, G.J.; Wang, G.; Huang, S. High performance PbS colloidal quantum dot solar cells by employing solution-processed CdS thin films from a single-source precursor as the electron transport layer. *Adv. Funct. Mater.* **2017**, *27*, 1–7. [CrossRef]
218. Tang, J.; Liu, H.; Zhitomirsky, D.; Hoogland, S.; Wang, X.; Furukawa, M.; Levina, L.; Sargent, E.H. Quantum junction solar cells. *Nano Lett.* **2012**, *12*, 4889–4894. [CrossRef] [PubMed]
219. Ning, Z.; Zhitomirsky, D.; Adinolfi, V.; Sutherland, B.; Xu, J.; Voznyy, O.; Maraghechi, P.; Lan, X.; Hoogland, S.; Ren, Y.; et al. Graded doping for enhanced colloidal quantum dot photovoltaics. *Adv. Mater.* **2013**, *25*, 1719–1723. [CrossRef] [PubMed]
220. Jeong, K.S.; Deng, Z.; Keuleyan, S.; Liu, H.; Guyot-Sionnest, P. Air-stable n-doped colloidal HgS quantum dots. *J. Phys. Chem. Lett.* **2014**, *5*, 1139–1143. [CrossRef] [PubMed]
221. Weidman, M.C.; Beck, M.E.; Hoffman, R.S.; Prins, F.; Tisdale, W.A. Monodisperse, air-stable PbS nanocrystals via precursor stoichiometry control. *ACS Nano* **2014**, *8*, 6363–6371. [CrossRef] [PubMed]
222. Zhang, J.; Gao, J.; Church, C.P.; Miller, E.M.; Luther, J.M.; Klimov, V.I.; Beard, M.C. PbSe quantum dot solar cells with more than 6% efficiency fabricated in ambient atmosphere. *Nano Lett.* **2014**, *14*, 6010–6015. [CrossRef] [PubMed]
223. Kim, S.; Marshall, A.R.; Kroupa, D.M.; Miller, E.M.; Luther, J.M.; Jeong, S.; Beard, M.C. Air-stable and efficient PbSe quantum-dot solar cells based upon ZnSe to PbSe cation-exchanged quantum dots. *ACS Nano* **2015**, *9*, 8157–8164. [CrossRef] [PubMed]
224. Zhang, Y.; Ding, C.; Wu, G.; Nakazawa, N.; Chang, J.; Ogomi, Y.; Toyoda, T.; Hayase, S.; Katayama, K.; Shen, Q. Air stable PbSe colloidal quantum dot heterojunction solar cells: Ligand-dependent exciton dissociation, recombination, photovoltaic property, and stability. *J. Phys. Chem. C* **2016**, *120*, 28509–28518. [CrossRef]
225. Zhang, Z.; Chen, Z.; Zhang, J.; Chen, W.; Yang, J.; Wen, X.; Wang, B.; Kobamoto, N.; Yuan, L.; Stride, J.A.; et al. Significant improvement in the performance of PbSe quantum dot solar cell by introducing a $CsPbBr_3$ perovskite colloidal nanocrystal back layer. *Adv. Energy Mater.* **2017**, *7*, 1–7.
226. Zhang, Y.; Wu, G.; Ding, C.; Liu, F.; Yao, Y.; Zhou, Y.; Wu, C.; Nakazawa, N.; Huang, Q.; Toyoda, T.; et al. Lead selenide colloidal quantum dot solar cells achieving high open-circuit voltage with one-step deposition strategy. *J. Phys. Chem. Lett.* **2018**, *9*, 3598–3603. [CrossRef] [PubMed]

227. Zhang, Z.; Chen, Z.; Yuan, L.; Chen, W.; Yang, J.; Wang, B.; Wen, X.; Zhang, J.; Hu, L.; Stride, J.A.; et al. A new passivation route leading to over 8% efficient PbSe quantum-dot solar cells via direct ion exchange with perovskite nanocrystals. *Adv. Mater.* **2017**, *29*, 1–8. [CrossRef] [PubMed]
228. Kim, T.; Gao, Y.; Hu, H.; Yan, B.; Ning, Z.; Jagadamma, L.K.; Zhao, K.; Kirmani, A.R.; Eid, J.; Adachi, M.M.; et al. Hybrid tandem solar cells with depleted-heterojunction quantum dot and polymer bulk heterojunction subcells. *Nano Energy* **2015**, *17*, 196–205. [CrossRef]
229. Futscher, M.H.; Ehrler, B. Modeling the performance limitations and prospects of perovskite/si tandem solar cells under realistic operating conditions. *ACS Energy Lett.* **2017**, *2*, 2089–2095. [CrossRef] [PubMed]
230. Gao, J.; Luther, J.M.; Semonin, O.E.; Ellingson, R.J.; Nozik, A.J.; Beard, M.C. Quantum dot size dependent *J–V* characteristics in heterojunction ZnO/PbS quantum dot solar cells. *Nano Lett.* **2011**, *11*, 1002–1008. [CrossRef] [PubMed]
231. Gao, J.; Perkins, C.L.; Luther, J.M.; Hanna, M.C.; Chen, H.-Y.; Semonin, O.E.; Nozik, A.J.; Ellingson, R.J.; Beard, M.C. N-type transition metal oxide as a hole extraction layer in PbS quantum dot solar cells. *Nano Lett.* **2011**, *11*, 3263–3266. [CrossRef] [PubMed]
232. Brown, P.R.; Lunt, R.R.; Zhao, N.; Osedach, T.P.; Wanger, D.D.; Chang, L.-Y.; Bawendi, M.G.; Bulović, V. Improved current extraction from ZnO/PbS quantum dot heterojunction photovoltaics using a MoO_3 interfacial layer. *Nano Lett.* **2011**, *11*, 2955–2961. [CrossRef] [PubMed]
233. Neo, D.C.J.; Zhang, N.; Tazawa, Y.; Jiang, H.; Hughes, G.M.; Grovenor, C.R.M.; Assender, H.E.; Watt, A.A.R. Poly(3-hexylthiophene-2,5-diyl) as a hole transport layer for colloidal quantum dot solar cells. *ACS Appl. Mater. Interfaces* **2016**, *8*, 12101–12108. [CrossRef] [PubMed]
234. Swarnkar, A.; Marshall, A.R.; Sanehira, E.M.; Chernomordik, B.D.; Moore, D.T.; Christians, J.A.; Chakrabarti, T.; Luther, J.M. Quantum dot-induced phase stabilization of α-$CsPbI_3$ perovskite for high-efficiency photovoltaics. *Science* **2016**, *354*, 92–95. [CrossRef] [PubMed]
235. Wheeler, L.M.; Sanehira, E.M.; Marshall, A.R.; Schulz, P.; Suri, M.; Anderson, N.C.; Christians, J.A.; Nordlund, D.; Sokaras, D.; Kroll, T.; et al. Targeted ligand exchange chemistry on cesium lead halide perovskite quantum dots for high-efficiency photovoltaics. *J. Am. Chem. Soc.* **2018**, *140*, 10504–10513. [CrossRef] [PubMed]
236. Sanehira, E.M.; Marshall, A.R.; Christians, J.A.; Harvey, S.P.; Ciesielski, P.N.; Wheeler, L.M.; Schulz, P.; Lin, L.Y.; Beard, M.C.; Luther, J.M. Enhanced mobility $CsPbI_3$ quantum dot arrays for record-efficiency, high-voltage photovoltaic cells. *Sci. Adv.* **2017**, *3*, eaao4204. [CrossRef] [PubMed]
237. Chuang, C.-H.M.; Maurano, A.; Brandt, R.E.; Hwang, G.W.; Jean, J.; Buonassisi, T.; Bulović, V.; Bawendi, M.G. Open-circuit voltage deficit, radiative sub-bandgap states, and prospects in quantum dot solar cells. *Nano Lett.* **2015**, *15*, 3286–3294. [CrossRef] [PubMed]
238. Marshall, A.R.; Young, M.R.; Nozik, A.J.; Beard, M.C.; Luther, J.M. Exploration of metal chloride uptake for improved performance characteristics of PbSe quantum dot solar cells. *J. Phys. Chem. Lett.* **2015**, *6*, 2892–2899. [CrossRef] [PubMed]
239. Erslev, P.T.; Chen, H.-Y.; Gao, J.; Beard, M.C.; Frank, A.J.; van de Lagemaat, J.; Johnson, J.C.; Luther, J.M. Sharp exponential band tails in highly disordered lead sulfide quantum dot arrays. *Phys. Rev. B* **2012**, *86*, 155313. [CrossRef]
240. Jean, J.; Mahony, T.S.; Bozyigit, D.; Sponseller, M.; Holovsky, J.; Bawendi, M.G.; Bulovic, V. Radiative efficiency limit with band tailing exceeds 30% for quantum dot solar cells. *ACS Energy Lett.* **2017**, *2*, 2616–2624. [CrossRef]
241. Nagpal, P.; Klimov, V.I. Role of mid-gap states in charge transport and photoconductivity in semiconductor nanocrystal films. *Nat. Commun.* **2011**, *2*, 486. [CrossRef] [PubMed]
242. Bozyigit, D.; Lin, W.M.M.; Yazdani, N.; Yarema, O.; Wood, V. A quantitative model for charge carrier transport, trapping and recombination in nanocrystal-based solar cells. *Nat. Commun.* **2015**, *6*, 6180. [CrossRef] [PubMed]
243. Marino, E.; Kodger, T.E.; Hove, J.B.t.; Velders, A.H.; Schall, P. Assembling quantum dots via critical casimir forces. *Sol. Energy Mater. Sol. Cells* **2016**, *158*, 154–159. [CrossRef]
244. Marino, E.; Kodger, T.E.; Wegdam, G.H.; Schall, P. Revealing driving forces in quantum dot supercrystal assembly. *Adv. Mater.* **2018**, 1803433. [CrossRef] [PubMed]

245. Evers, W.H.; Schins, J.M.; Aerts, M.; Kulkarni, A.; Capiod, P.; Berthe, M.; Grandidier, B.; Delerue, C.; van der Zant, H.S.J.; van Overbeek, C.; et al. High charge mobility in two-dimensional percolative networks of PbSe quantum dots connected by atomic bonds. *Nat. Commun.* **2015**, *6*, 8195. [CrossRef] [PubMed]
246. Kulkarni, A.; Evers, W.H.; Tomić, S.; Beard, M.C.; Vanmaekelbergh, D.; Siebbeles, L.D.A. Efficient steplike carrier multiplication in percolative networks of epitaxially connected PbSe nanocrystals. *ACS Nano* **2017**, *12*, 378–384. [CrossRef] [PubMed]
247. van Overbeek, C.; Peters, J.L.; van Rossum, S.A.P.; Smits, M.; van Huis, M.A.; Vanmaekelbergh, D. Interfacial self-assembly and oriented attachment in the family of PbX (X = S, Se, Te) nanocrystals. *J. Phys. Chem. C* **2018**, *122*, 12464–12473. [CrossRef] [PubMed]
248. Boles, M.A.; Engel, M.; Talapin, D.V. Self-assembly of colloidal nanocrystals: From intricate structures to functional materials. *Chem. Rev.* **2016**, *116*, 11220–11289. [CrossRef] [PubMed]
249. Gómez-Campos, F.M.; Rodríguez-Bolívar, S.; Califano, M. High-mobility toolkit for quantum dot films. *ACS Photonics* **2016**, *3*, 2059–2067. [CrossRef]
250. André, A.; Weber, M.; Wurst, K.M.; Maiti, S.; Schreiber, F.; Scheele, M. Electron-conducting PbS nanocrystal superlattices with long-range order enabled by terthiophene molecular linkers. *ACS Appl. Mater. Interfaces* **2018**, *10*, 24708–24714. [CrossRef] [PubMed]

© 2018 by the authors. Licensee MDPI, Basel, Switzerland. This article is an open access article distributed under the terms and conditions of the Creative Commons Attribution (CC BY) license (http://creativecommons.org/licenses/by/4.0/).